RSC Advances

PAPER

View Article Online
View Journal | View Issue

Cite this: *RSC Adv.*, 2026, **16**, 9590

Pyrazolo[3,4-*d*]pyrimidine derivatives as VEGFR-2 and EGFR^{T790M} dual inhibitors: design, docking, ADMET, synthesis and anticancer evaluations

Nada A. A. M. Aziz,*[ab] Riham F. George,[c] Tamer Nasr,[de] Khaled El-Adl*[bf] and Ghada F. Elmasry*[c]

Novel pyrazolo[3,4-*d*]pyrimidine derivatives have been designed, synthesized and examined as inhibitors of both EGFR^{T790M} and VEGFR-2. These compounds exhibit anticancer activities against HCT-116, MCF-7, HepG2 and A549 cancer cell lines. Docking studies were carried out to identify how the proposed molecules interact with both VEGFR-2 and EGFR^{T790M}. The results of the docking studies showed excellent correlation with the biological screening results. Derivatives **7c**, **8b**, **7e** and **8c** exhibit very good anticancer activities against A549, with IC_{50} values of 5.75, 6.20, 6.55 and 7.10 μM, respectively. Molecules **7c**, **8b**, **7e**, **8c**, **7d** and **7b** showed IC_{50} values of 5.50, 5.80, 6.15, 7.00, 9.40 and 9.50 μM, respectively, against HCT-116, establishing remarkable anticancer activities, while derivatives **7c**, **8b**, **7e** and **8c** showed potent anticancer activities against MCF-7, with IC_{50} values of 5.90, 6.40, 7.00 and 7.90 μM, respectively. Moreover, molecules **7c**, **8b**, **7e** and **8c**, with corresponding IC_{50} values of 5.00, 5.30, 5.75 and 8.80 μM, demonstrated the highest anticancer activities against HepG2. The particularly active molecules **7b**, **7c**, **7d**, **7e**, **8b** and **8c** were tested against VERO normal cell lines, and their low toxicity was established by IC_{50} values ranging from 40.00 to 53.99 μM. Furthermore, all the derivatives were studied as inhibitors of both EGFR^{T790M} and VEGFR-2. Molecules **7c**, **8b**, **7e** and **8c**, with IC_{50} values ranging from 0.90 to 1.25 μM, exhibited very good inhibition against VEGFR-2. In addition, molecules **7c**, **8b**, **7e**, **7b** and **8c**, with IC_{50} values of 0.25, 0.32, 0.35, 0.45 and 0.50 μM, respectively, displayed very good EGFR^{T790M} inhibition. Furthermore, molecules **7c**, **7e** and **8b** exhibited excellent ADMET profile compared to sorafenib and erlotinib.

Received 2nd January 2026
Accepted 2nd February 2026

DOI: 10.1039/d6ra00037a

rsc.li/rsc-advances

1. Introduction

Cancer cells can develop new blood vessels to receive nutrients and oxygen from the neighboring cells. Thus, cancer can spread to other organs, mainly the liver, lung, and bones, through blood vessels and lymphatic systems.[1–4] Inhibition of VEGFR-2 (vascular endothelial growth factor receptor) and EGFR (epidermal growth factor receptor) is crucial for the prevention of tumor metastasis, angiogenesis, and tumor growth.[5,6] The two pathways have comparable signaling routes. VEGF expression and angiogenesis are reduced upon EGFR inhibition. Moreover, elevated VEGFR-2 levels in turn, contribute to the development of resistance to EGFR inhibitors.[7] EGFR-mutant cancers are influenced by VEGF more than EGFR wild-type tumors.[8] In nearly 90% of cases, EGFR-mutant NSCLC tumors harbor an exon 21 L858R mutation or an exon 19 deletion, both of which make tumors sensitive to EGFR TKIs in patients.[9] In the metastatic setting, EGFRTKIs have been recognized as a first-line therapy because of their excellent tolerability and progression-free survival (PFS) benefits.[10] Dual concurrent inhibition of VEGFR-2 and EGFR succeeded by working synergistically to target and treat cancer cells.[11] An ATP-binding site is present in both the enzymes, which permits a number of small molecules to bind powerfully and act as dual inhibitors, including afatinib (VI), lapatinib (V), vandetanib (IV), sorafenib (III), gefitinib (II), and erlotinib (I) (Fig. 1).[12] Most of these small molecules consist of quinazoline-based structures, and many challenges have been overcome to modify their structure in order to produce more active anticancer agents. Therefore, the search for new structures that can act as inhibitors of tyrosine kinase continues.[13–16]

[a]*Postgraduate program in Pharmaceutical Chemistry, Faculty of Pharmacy, Cairo University, Cairo, Egypt. E-mail: nada.aziz@hu.edu.eg*

[b]*Pharmaceutical Chemistry Department, Faculty of Pharmacy, Heliopolis University for Sustainable Development, Cairo, Egypt*

[c]*Pharmaceutical Chemistry Department, Faculty of Pharmacy, Cairo University, Cairo, Egypt. E-mail: ghada.elmasry@pharma.cu.edu.eg*

[d]*Department of Pharmaceutical Chemistry, Faculty of Pharmacy, Capital University (Formerly Helwan University), Ain-Helwan, Cairo 11795, Egypt*

[e]*Medicinal Chemistry Department, Faculty of Pharmacy, Egypt-Japan University of Science and Technology (E-JUST), P.O. 21934, Alexandria, Egypt*

[f]*Pharmaceutical Medicinal Chemistry & Drug Design Department, Faculty of Pharmacy (Boys), Al-Azhar University, Cairo 11884, Egypt. E-mail: eladlkhaled74@azhar.edu.eg; khaled.eladl@hu.edu.eg; eladlkhaled74@yahoo.com*

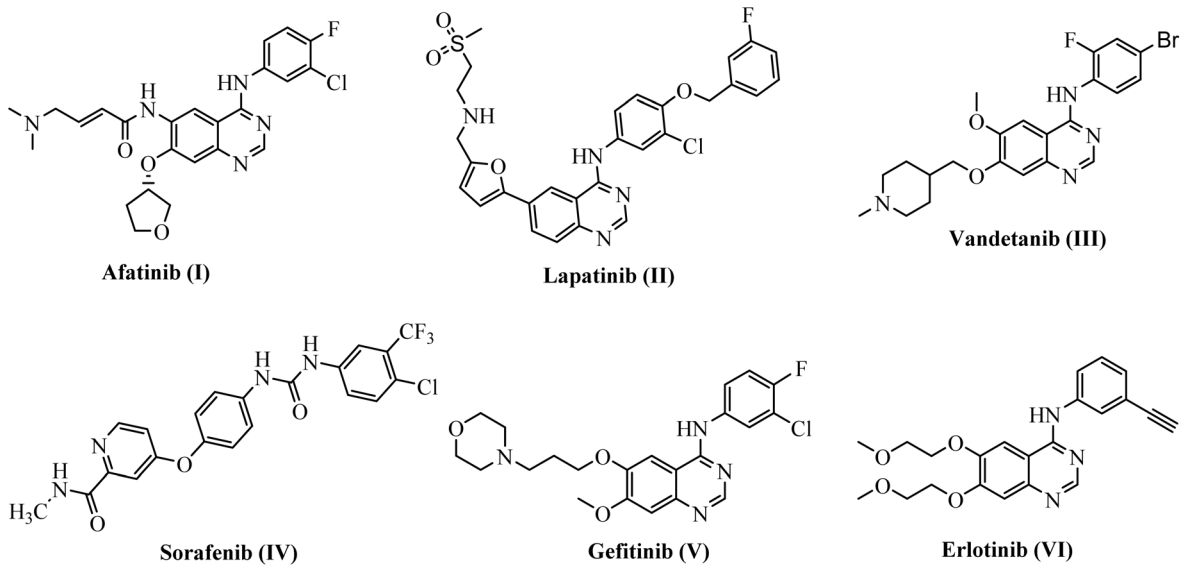

Fig. 1 Reported dual VEGFR-2 and EGFR inhibitors.

The fused pyrazolo[3,4-*d*]pyrimidine ring has received much consideration due to its molecular similarity to purines and its broad range of pharmacological potential.[1,17] In the literature, this scaffold has been shown to exhibit anticancer effects through a diverse set of pathways.[1,17–19] Pyrazolo[3,4-*d*]pyrimidine derivatives have been reported to have anticancer activities as inhibitors of EGFR, VEGFR-2,[20,21] dihydrofolate reductase (DHFR),[22] mitogen-activated protein (MAP) kinase,[23] protein kinase target platelet-derived growth factor receptor (PDGFR), and Aurora-A.[21] These results motivate us to evaluate our novel molecules as dual VEGFR-2 and EGFR inhibitors.

VEGFR-2 inhibitors can be categorized into three main classes. Class I inhibits the ATP region and forms one H-bond with Cys919 in the hinge region. Class II also inhibits the ATP region, but extends beyond the gate region, and inhibits the allosteric hydrophobic pocket. Class III inhibits the allosteric hydrophobic pocket. The specificity and affinity of Class II inhibitors make them superior to Class I and III inhibitors[24] (Fig. 2A).

Moreover, the ATP-binding site of EGFR-TK has five key areas. (a) A phosphate-binding area that is used to enhance the inhibitor's pharmacokinetics. (b) A hydrophobic area I, which has an important role in selectivity and inhibition. (c) A hydrophobic area II, which is employed for inhibition activity. (d) A hydrophilic ribose sugar area, and (e) an adenine binding area, which includes the adenine ring and significant amino acids that form hydrogen bonds[25] (Fig. 2B).

In line with our previous work,[26–40] we continue to synthesize and develop new anticancer agents. Therefore, we designed and synthesized new pyrazolo[3,4-*d*]pyrimidines as dual inhibitors of EGFR-mutant/VEGFR-2. These molecules can be used as antiproliferative agents against HCT-116, MCF-7, HepG2 and A549 cell lines in which VEGFR-2/EGFR-mutants are over-expressed.

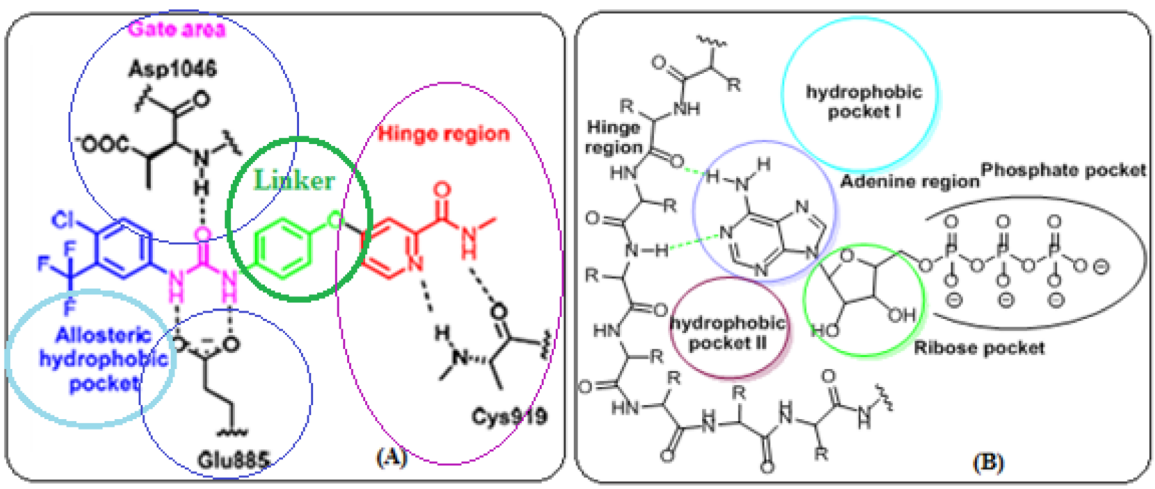

Fig. 2 (A) VEGFR-2 binding site. (B) EGFR-TK binding site.

1.1. Rationale and structure-based design

Our novel molecules showed the essential structure requirements for both VEGFR-2 and EGFR inhibitors (Fig. 3 and 4). Numerous VEGFR-2 inhibitors, including sorafenib, have four significant parts:[41,42] (i) A hydrophobic tail that inhibited the allosteric hydrophobic pocket.[43] (ii) A linker with HBA/HBD (H-bond acceptor/H-bond donor) groups that form H-bonds with Glu885 and Asp1046.[44] (iii) A central hydrophobic spacer.[45] (iv) A flat hetero aromatic ring that inhibited ATP-binding area.[42] Our VEGFR-2 inhibition design depends on bioisosteric replacement techniques based on sorafenib at four points (Fig. 3).

The main technique is to use the 6-methyl-1-phenyl-pyrazolo [3,4-*d*]pyrimidine heteroaromatic scaffold to inhibit the ATP region. The second modification is to use phenyl linkers. The third modification is to use formamide spacers to inhibit the gate area. Lastly, the fourth modification is to use an aliphatic and/or aromatic hydrophobic tail to inhibit the allosteric hydrophobic pocket. The elongation of the structure allows our molecules to be considered as Class II VEGFR-2 inhibitors, as they can inhibit the ATP area and extend outside the gate region and inhibit the allosteric hydrophobic pocket (Fig. 3).

On the other hand, EGFR-TKIs, including erlotinib, also have four significant parts. (i) A heteroaromatic structure that inhibits the adenine area.[46] (ii) A HBA/HBD spacer, *e.g.* NH group, that forms H-bonds with the amino acids in the linker

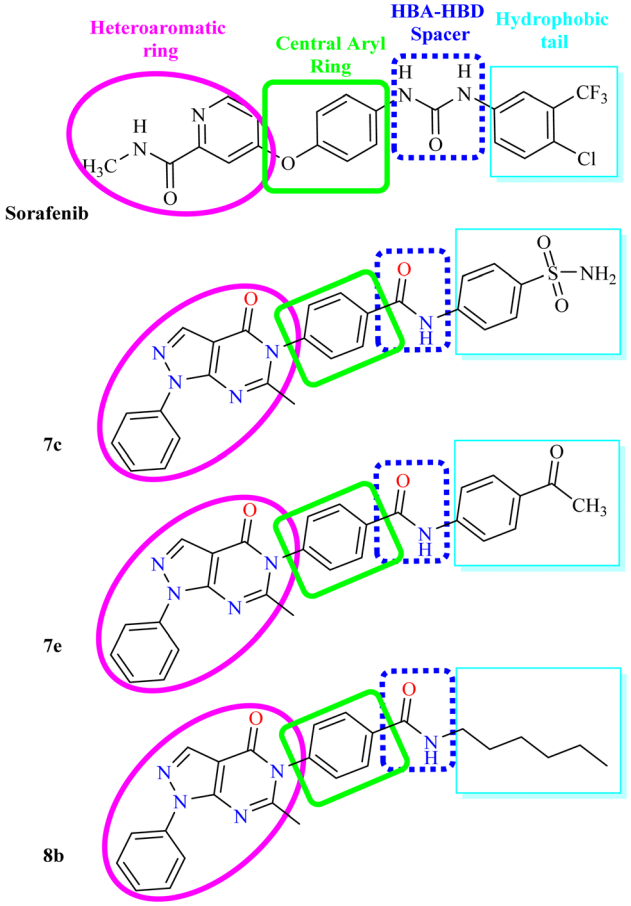

Fig. 3 Structural features of VEGFR-2 inhibitors.

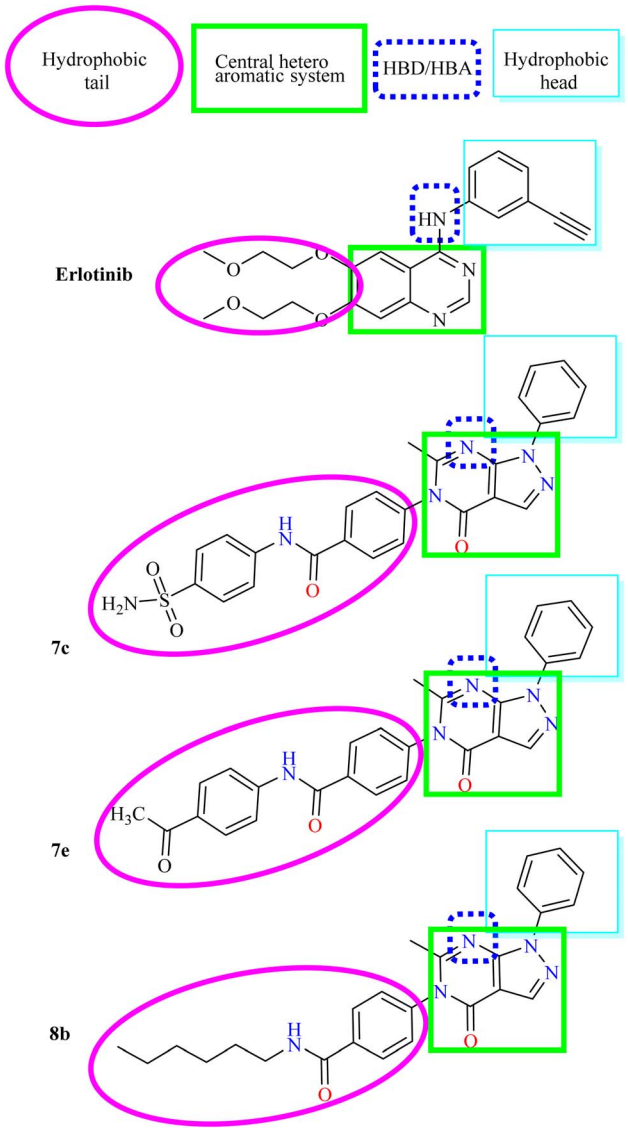

Fig. 4 Structural features of EGFR inhibitors.

area. (iii) A hydrophobic domain that inhibits the hydrophobic head I. (iv) A hydrophobic tail that inhibits the hydrophobic pocket II[47] (Fig. 4).

Our pyrazolopyrimidine molecules with elongated structures contain the basic pharmacophoric characteristics of EGFR-TKIs. Pyrazolopyrimidines replaced the heteroaromatic quinazoline of erlotinib and inhibited the adenine-binding area. Secondly, the 2-methoxyethoxy groups (hydrophobic tail) were replaced with the elongated side chains at position-5 of pyrazolopyrimidine to inhibit the hydrophobic pocket II. Thirdly, the *N* at position-7 of pyrazolopyrimidine was used as a hydrogen-bond acceptor (HBA). The phenyl ring at position-1 of pyrazolopyrimidine was the fourth modification (hydrophobic head) (Fig. 4).

All of these modifications stimulated our team to investigate the structure–activity relationship (SAR) of the prepared molecules, which served as anticancer agents with $EGFR^{T790M}$ and VEGFR-2 dual inhibition.

2. Results and discussion

2.1. Chemistry

The targeted molecules **5**, **6**, **7a–e** and **8a–c** were gained by following the steps shown in Schemes 1 and 2. Production was started by condensation of ethyl 2-cyanoacetate and triethylorthoformate in the presence of acetic anhydride to give ethyl 2-cyano-3-ethoxyacrylate (**1**), which underwent an additional cyclization reaction with phenylhydrazine[48] to give ethyl 5-amino-1-phenyl-1*H*-pyrazole-4-carboxylate **2**. Consequent stirring of **2** with alcoholic 10% potassium hydroxide solution gave 5-amino-1-phenyl-1*H*-pyrazole-4-carboxylic acid **3**.[49] Acetylation and consequent condensation of **3** in acetic anhydride afforded 6-methyl-1-phenylpyrazolo[3,4-*d*][1,3] oxazin-4(1*H*)-one **4**,[49] which was treated with *p*-aminobenzoic acid and/or ethyl *p*-aminobenzoate to yield the respective derivatives **5** and **6** (Scheme 1). Constant stirring of the benzoic acid derivative **5** with ECF (ethyl chloroformate) in the presence of DMF and TEA, followed by the addition of suitable aliphatic and aromatic amines, produced the respective amides **7a–e** and **8a–c**, by following the mixed anhydride method[34] (Scheme 2).

The ^{1}H NMR spectrum of compound **7d** showed the appearance of two new singlet signals corresponding to the (OCH_3) and NH groups at 3.76 and 10.30 ppm, respectively. In addition, compound **7e** showed two new singlet signals corresponding to ($COCH_3$) and NH groups at 2.57 and 10.73 ppm,

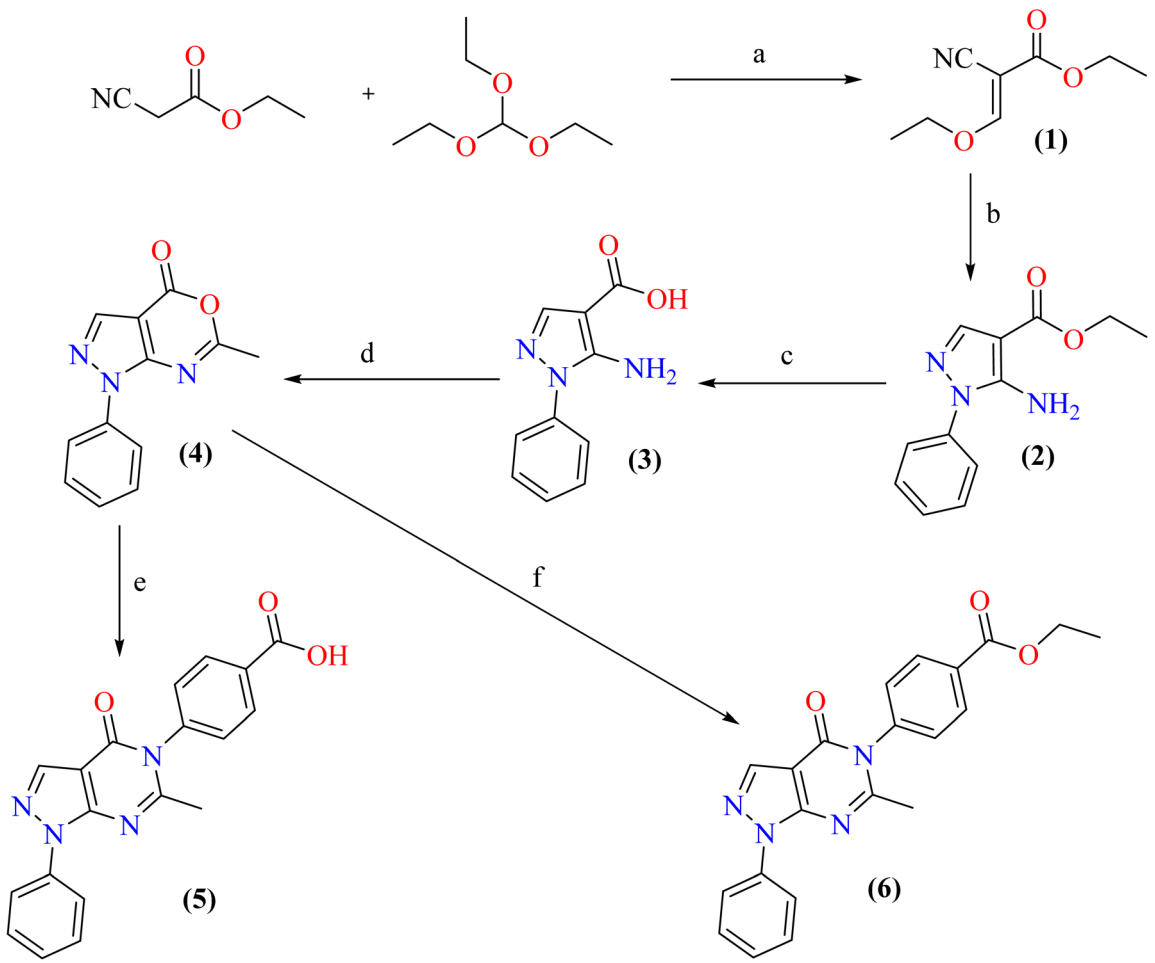

Reagents and conditions
a) Acetic anhydride / reflux;
b) Phenylhydrazine / reflux;
c) NaOH / Ethanol / reflux;
d) Acetic anhydride / reflux;
e) Acetic acid glacial / NH_2-C_6H_4-(4-COOH) / reflux
f) Acetic acid glacial / NH_2-C_6H_4-(4-$COOC_2H_5$) / reflux

Scheme 1 Synthetic steps for the targeted compounds **5** and **6**.

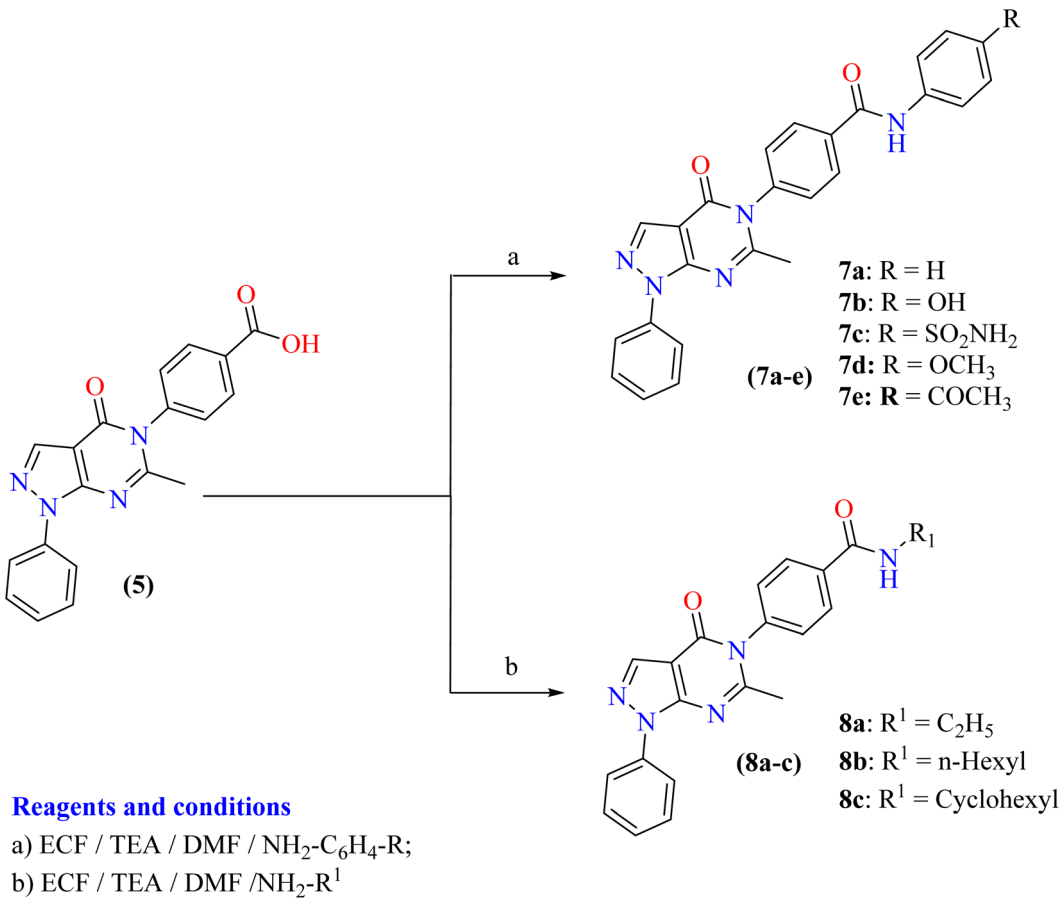

Scheme 2 Synthetic scheme for the synthesis of the targeted compounds 7a–e and 8a–c.

respectively. Moreover, the mass spectrum for compound **7e** showed the molecular ion peak at *m*/*z* 463.03, corresponding to its molecular weight. The ^{1}H NMR spectrum of compound **8c** showed new signals at 1.10–3.79 ppm attributed to the cyclohexyl protons. In addition, the ^{13}C NMR spectrum showed characteristic signals corresponding to its structure. Moreover, the mass spectrum for compound **8c** showed a molecular ion peak at *m*/*z* 427.34, corresponding to its molecular weight.

2.2. Docking studies

For molecular docking investigations, MolSoft software was used. The PDB IDs for VEGFR-2 (PDB ID 4ASD)[50–52] and EGFR^{T790M} (PDB ID 3W2O)[43] were used in each experiment.

2.2.1. Docking studies using VEGFR-2 inhibitors. Sorafenib bound in an orientation with a ΔG of −99.50 kcal mol^{-1} and exhibited 5 H-bonds with Cys919 (2.51 Å and 2.10 Å), Glu885 (1.77 Å and 2.75 Å), and Asp1046 (1.50 Å). The *N*-methylpicolinamide group occupied and inhibited the hydrophobic pocket generated by Leu840, Val848, Glu917, Lys920, Leu1035, Phe918, and Cys919. Moreover, the central phenoxy linker occupied and inhibited the hydrophobic channel generated by Val848, Lys868, Thr916, Leu1035 and Cys1045. Additionally, the 3-triflurometh-4-chlorophenyl tail occupied and inhibited the allosteric hydrophobic channel generated by Glu885, Ile892, Ile888, Hie1026, Asp1046 and Cys1045 (Fig. 5). The urea spacer plays a fundamental role in the high binding affinity of sorafenib with VEGFR-2. These results encouraged us to experiment with formamide linkers in order to gain more effective VEGFR-2 inhibitors.

The binding orientation of compound **7c** is nearly the same as that of sorafenib. It showed a ΔG of −105.02 kcal mol^{-1} (Table 1) and 6 H-bonds with Cys919 (2.15 Å), Asp1046 (2.23 Å and 2.96 Å), Glu885 (2.98 Å), Ile1025 (1.59 Å) and Hie1026 (2.56 Å). The pocket formed by Leu840, Val848, Glu917, Phe918, Cys919, Lys920 and Leu1035 was occupied and inhibited by the 1-phenylpyrazolopyrimidine scaffold. Additionally, the hydrophobic channel generated by Glu885, Ile888, Ile892, Hie1026 and Ile1025 was occupied and inhibited by the terminal benzenesulfonamide tail (Fig. 6). The strongest anticancer activity of compound **7c** may be explained by these interactions.

The binding orientation of compound **8b** is nearly the same as that of **7c**. It showed a binding energy of −101.13 kcal mol^{-1} and 4 H-bonds with Cys919 (1.92 Å), Asp1046 (2.19 Å and 2.95 Å) and Glu885 (2.97 Å) (Fig. 7). In addition, compound **7e** bound in a favorable orientation, with a binding energy of-93.63 kcal mol^{-1} and forming four H-bonds (Fig. 8).

2.2.2. Docking as EGFR^{T790M} inhibitors. Erlotinib adopted a binding orientation with a binding energy of −82.77 kcal mol^{-1} (Table 2) and four H-bonds with Thr854 (2.99 Å), Met793 (1.82 Å), Val726 (2.97 Å) and Cys797 (2.05 Å). The

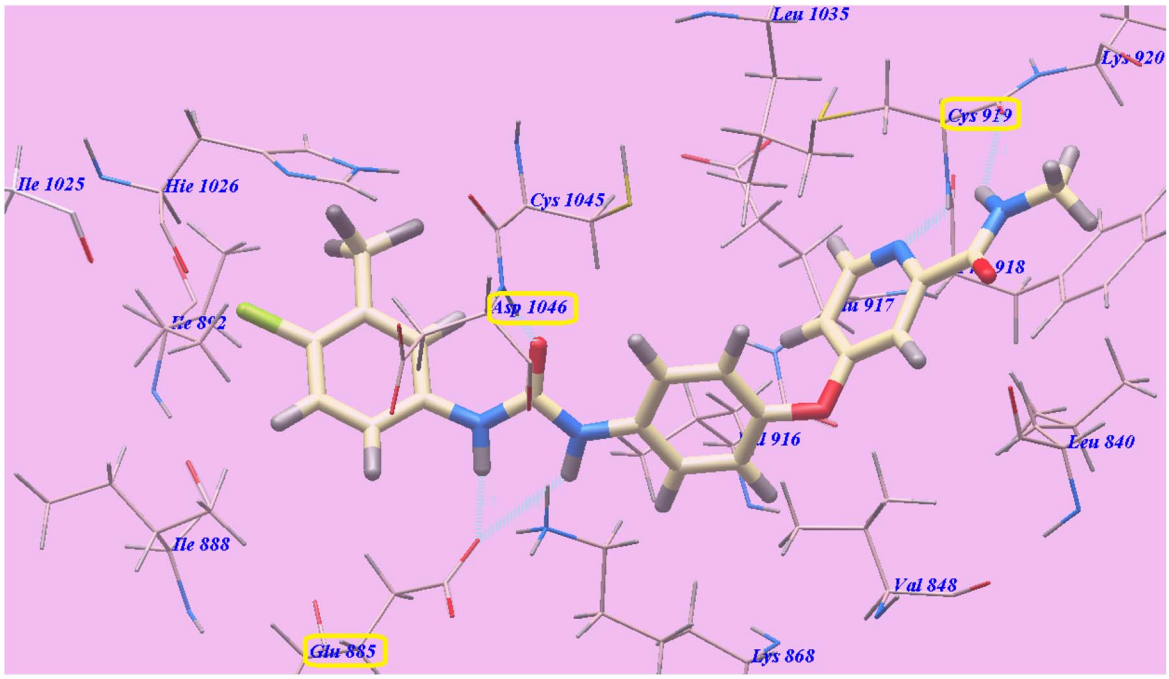

Fig. 5 Sorafenib binding orientation with 4ASD. Dotted lines represent H-bonds.

hydrophobic area I, which is generated by Phe723, Ile759, Thr854, Glu762, Leu777, Met790, Glu791, Asp855, and Val726, was occupied and inhibited by the 3-ethynylphenyl head. Additionally, the 2-methoxyethoxy tail occupied and inhibited the hydrophobic area II generated by Leu718, Met793, Pro794, Leu844 and Val845 (Fig. 9).

The binding orientation of compound **7c** is nearly identical to that of erlotinib. It presented a binding energy of -97.48 kcal mol^{-1} and 5 H-bonds with Thr854 (2.98 Å), Gln791 (2.96 Å), Pro794 (2.54 Å) and Met793 (2.20 Å and 2.95 Å). The long side-chain occupied and inhibited the hydrophobic area II, generated by Leu718, Met793, Leu844, Pro794, Cys797, Val845, Gly724, Gln791, Met790, and Val726. The 1-phenyl-pyrazolopyrimidine occupied and inhibited hydrophobic area I, generated by Glu762, Leu777, Ile759, Leu788, Met790, Gly724, Thr854, Asp855, Glu758, and Phe723 (Fig. 10).

Compounds **8b** and **7e** adopt binding orientations that are almost identical to those of erlotinib and **7c**, with binding

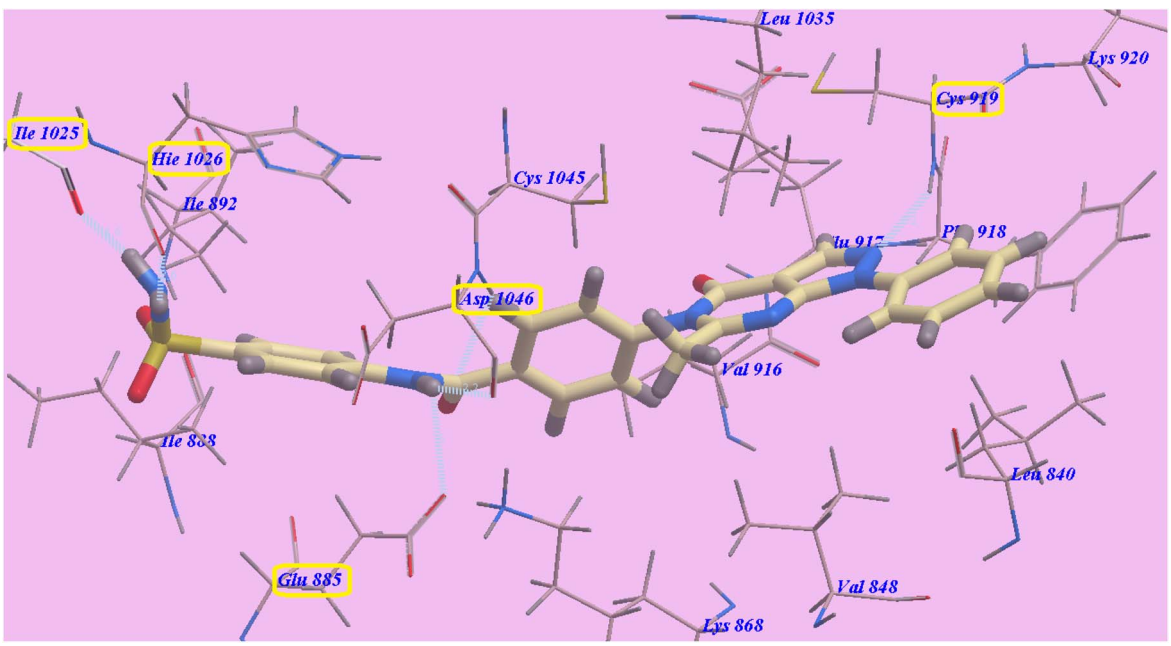

Fig. 6 Binding orientation of **7c** with 4ASD.

Table 1 Calculated free energy (ΔG in kcal mol^{-1}) for ligand binding with VEGFR-2

Compound	ΔG [kcal mol^{-1}]	Compound	ΔG [kcal mol^{-1}]
5	−65.11	**7e**	−93.63
6	−76.93	**8a**	−77.15
7a	−83.51	**8b**	−101.13
7b	−89.84	**8c**	−84.87
7c	−105.02	Sorafenib	−99.50
7d	−84.37		

energies of −86.17 kcal mol^{-1} (with four H-bonds formed; Fig. 11) and −81.85 kcal mol^{-1} (with 4 H-bonds formed; Fig. 12), respectively.

2.3. Molecular dynamics simulations

Molecular dynamics (MD) simulations were performed for the highly active molecules **7c**, **7e**, **8b** and **8c** in EGFR^{T790M} and VEGFR-2 proteins. The ligand-receptor binding energy was determined by employing Amber's MM/GBSA.py script and the trajectory.[53] Erlotinib and sorafenib were used as the respective positive controls. With the help of GAFF2 (ref. 54 and 55) and the AMBERff14SB protein force field, ligand force fields were produced.[56] The observed root mean square deviation (RMSD) confirmed the stability of the studied molecules as inhibitors within the defined active sites throughout the 50 ns all-atom MD runs (Fig. 13). Molecular divergence of a given ligand from the recognized original/reference structure is assessed by RMSD. The selected MD simulation procedure was valid, and it gave a respectable suggestion of the stability of the ligand-target interactions.

2.4. *In vitro* cytotoxic activity

The novel molecules **5**, **6**, **7a–e** and **8a–c** were tested against MCF-7, HepG2, HCT-116, A549 and VERO cell lines using the MTT protocol.[57–60] MCF-7, HepG2, HCT-116, A549 and VERO cell lines were obtained from the American Type Culture Collection (ATCC, Manassas, USA). Sorafenib and erlotinib were used as reference cytotoxic drugs. The obtained growth inhibitory concentration (IC_{50}) values are shown in Table 3. The results showed that most of the obtained molecules exhibited good to weak IC_{50} values against the studied cancer cell lines.

Derivatives **7c**, **8b**, **7e** and **8c** exhibited very good anticancer effects, with IC_{50} values of 5.75, 6.20, 6.55 and 7.10 μM, respectively, against A549. Derivatives **6**, **7a**, **7b**, **7d** and **8a**, with IC_{50} values of 10.30–13.00 μM, showed good cytotoxicity. Lastly, derivative **5** exhibited a moderate anticancer effect, with IC_{50} = 17.20 μM.

Derivatives **7c**, **8b**, **7e**, **8c**, **7d** and **7b** exhibited IC_{50} values of 5.50, 5.80, 6.15, 7.00, 9.40 and 9.50 μM, respectively, showing very good anticancer effects against HCT-116. Derivatives **6**, **7a** and **8a**, with IC_{50} values of 12.45, 10.70, and 10.25 μM, respectively, showed good cytotoxicity. Lastly, derivative **5** revealed a moderate anticancer effect, with IC_{50} = 16.30 μM.

Concerning MCF-7, derivatives **7c**, **8b**, **7e** and **8c** exhibited very good anticancer effects with IC_{50} values of 5.90, 6.40, 7.00 and 7.90 μM, respectively. Derivatives **6**, **7a**, **7b**, **7d** and **8a**, with IC_{50} values of 10.25–12.75 μM, showed good cytotoxicity. Lastly, derivative **5** revealed a moderate anticancer effect, with IC_{50} = 16.10 μM.

Regarding HepG2, derivatives **7c**, **8b**, **7e** and **8c**, with IC_{50} values of 5.00, 5.30, 5.75 and 8.80 μM, respectively, exhibited very good anticancer effects. Derivatives **6**, **7a**, **7b**, **7d** and **8a** showed good cytotoxicity, with IC_{50} = 10.50–14.70 μM. Lastly,

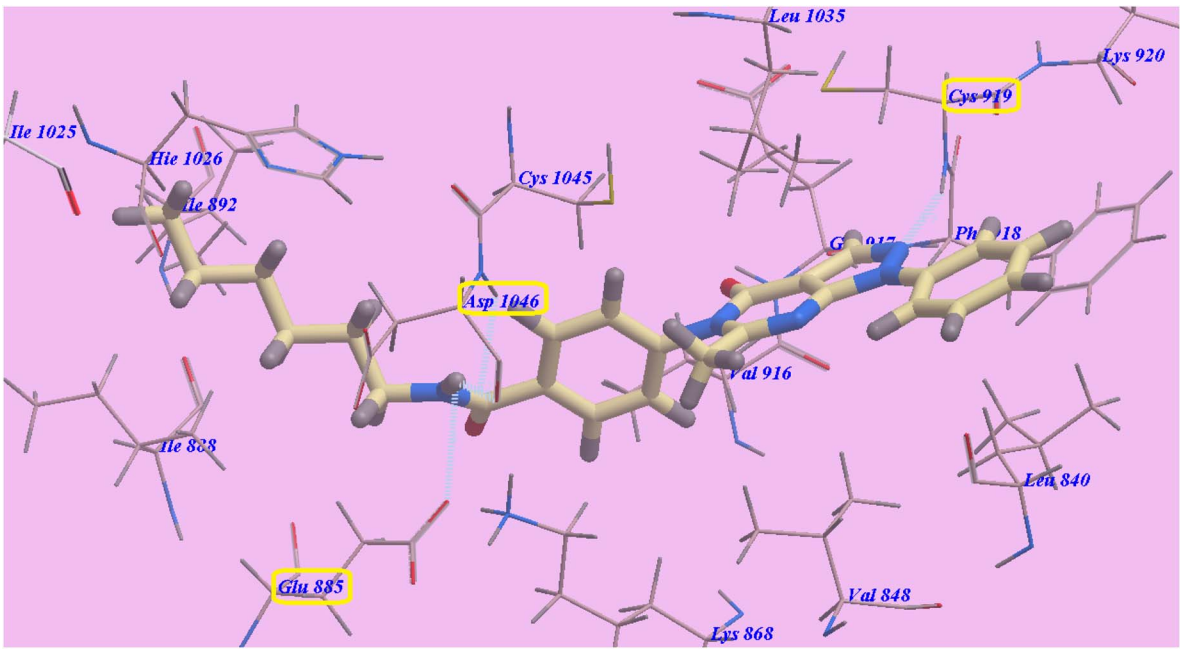

Fig. 7 Docking orientation of **8b** with 4ASD.

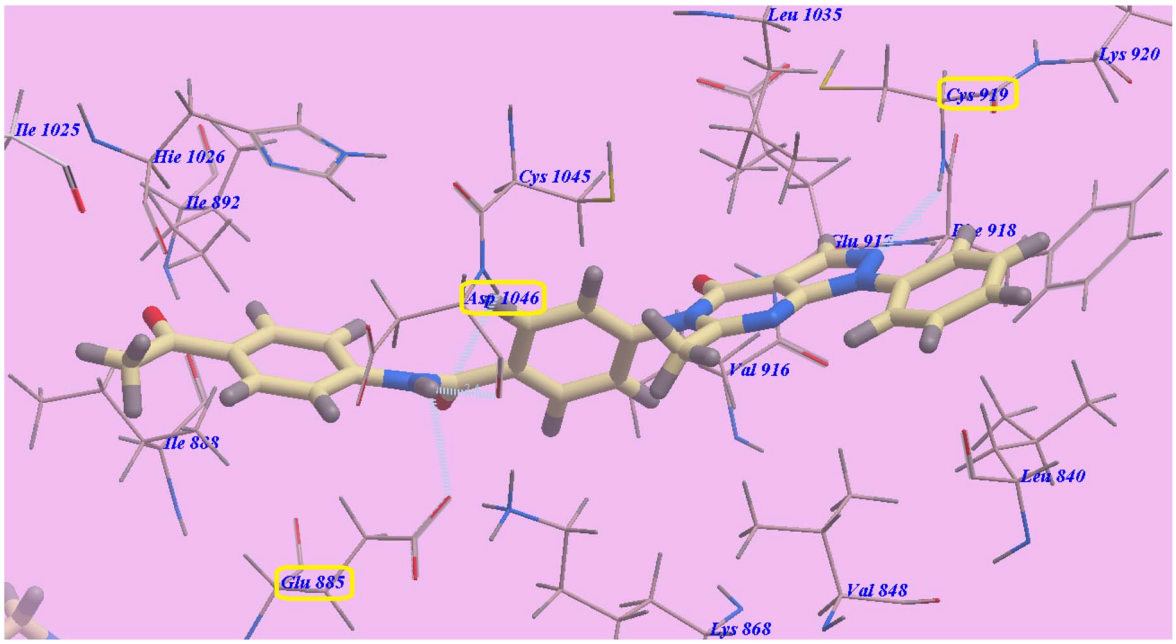

Fig. 8 Docking results for **7e** with 4ASD.

Table 2 Calculated free energy (ΔG in kcal mol^{-1}) for the binding of the synthesized compounds with EGFR^{T790M}

Compound	ΔG [kcal mol^{-1}]	Compound	ΔG [kcal mol^{-1}]
5	−61.84	**7e**	−81.85
6	−75.35	**8a**	−75.57
7a	−76.05	**8b**	−86.17
7b	−76.66	**8c**	−79.98
7c	−97.48	Erlotinib	−82.77
7d	−75.88		

derivative **5** revealed a moderate anticancer effect, with IC_{50} = 16.95 μM.

Ultimately, six highly potent molecules, **7b**, **7c**, **7d**, **7e**, **8b** and **8c**, were tested against VERO ordinary cell lines to evaluate their cytotoxic potential. The findings revealed that all the assessed agents possessed weak toxicity towards normal VERO cells, with IC_{50} values of 40.00–53.99 μM. One of the criteria for a good anti-cancer drug is that it should not affect non-cancerous cells. Molecules with low selectivity show SI <2, while those with moderate selectivity present SI values >2. A molecule with high selectivity typically exhibits SI values ≥5.[33] In this research, molecules **7b**, **7c**, **7d**, **7e**, **8b** and **8c** were respectively 4.57, 8.20, 5.03, 6.81, 8.71 and 5.63 times more toxic to A549 than to normal VERO cells and 4.96, 8.57, 5.61, 7.25, 9.31 and 5.71 times more lethal towards HCT-116 than to ordinary VERO cells. In addition, compounds **7b**, **7c**, **7d**, **7e**, **8b** and **8c** are respectively 4.60, 7.99, 5.15, 6.37, 8.44 and 5.06 times more toxic to MCF-7 than to normal VERO cells and 4.19, 9.43, 5.03, 7.76, 10.19 and 4.55 times more toxic to HepG2 than to ordinary VERO cells. All the molecules were highly selective against cancer cell lines, with SI values >5, except for molecule **7b**, which demonstrated moderate selectivity against the four cancer cells (SI = 4.19–4.96) and compound **8c** against HepG2 (SI = 4.55).

Moreover, molecules **7b**, **7c**, **7d**, **7e**, **8b** and **8c** are respectively 4.85, 8.49, 4.81, 7.24, 9.10 and 5.51 times more toxic towards A549 than to normal MCF-10 cells and 5.26, 8.87, 5.38, 7.72, 9.72 and 5.59 times more lethal to HCT-116 than to ordinary MCF-10 cells. In addition, compounds **7b**, **7c**, **7d**, **7e**, **8b** and **8c** are respectively 4.87, 8.27, 4.93, 6.78, 8.81 and 4.96 times more toxic to MCF-7 than to normal MCF-10 cells and 4.44, 9.76, 4.81, 8.25, 10.64 and 4.45 times more toxic to HepG2 than to ordinary MCF-10 cells. All molecules were highly selective against cancer cell lines, with SI values >5, except molecule **7b**, which demonstrated moderate selectivity against A549, MCF-7 and HepG2 cancer cells (SI = 4.85, 4.87 and 4.44, respectively) and compound **7d** against the same three cell lines (SI = 4.81, 4.93 and 4.81, respectively). In addition, derivative **8c** exhibited moderate selectivity against both MCF-7 and HepG2 cancer cells (SI = 4.96 and 4.45, respectively).

2.5. VEGFR-2 and EGFR^{T790M} kinases inhibitory assays

The Alpha Screen system (PerkinElmer, USA) using the anti-phosphotyrosine antibody was used to perform the VEGFR-2 inhibition assay with all molecules **5**, **6**, **7a–e** and **8a–c** (Table 4).[61] Sorafenib was used as the positive standard. The novel molecules exhibited different degrees of inhibition, with IC_{50} values of 0.90 to 2.90 μM. Derivatives **7c**, **8b**, **7e** and **8c**, with IC_{50} values of 0.90 to 1.25 μM, were the most active, with very good VEGFR-2 inhibition. Molecules **7a**, **7b** and **7d** exhibited good activity, with IC_{50} values of 1.50–1.95 μM. In addition, molecules **6** and **8a** exhibited moderate VEGFR-2 inhibition, with respective IC_{50} values of 2.55 and 2.15 μM. Finally, derivative **5**, with IC_{50} = 2.90 μM, exhibited the lowest VEGFR-2 inhibition.

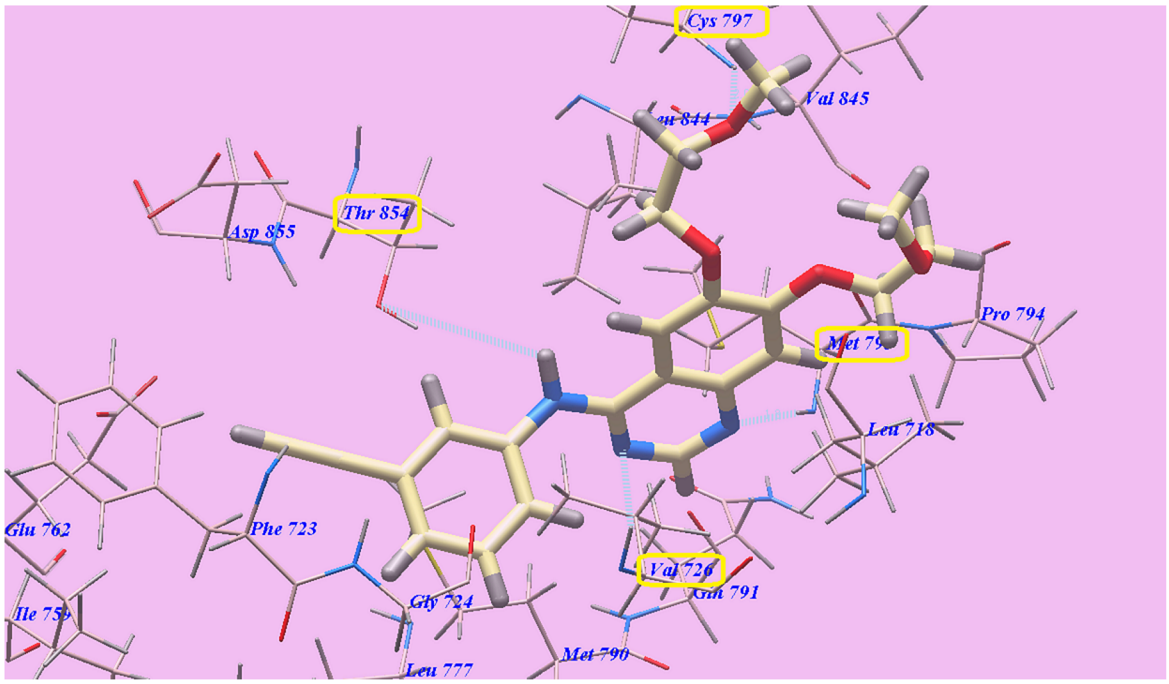

Fig. 9 Docking orientation of erlotinib with 3W2O, dotted lines represented H-bonds.

Furthermore, using the homogeneous time-resolved fluorescence (HTRF) technique,[62] the $EGFR^{T790M}$ inhibition assay was used to examine all the derivatives (**5**, **6**, **7a–e** and **8a–c**; Table 4). Erlotinib (IC_{50} = 0.24 μM) was employed as the standard. Very good $EGFR^{T790M}$ inhibition was achieved for compounds **7c**, **8b**, **7e**, **7b** and **8c**, with IC_{50} values 0.25, 0.32, 0.35, 0.45 and 0.50 μM, respectively. Furthermore, compound **7d**, with an IC_{50} of 0.60 μM, showed a good inhibition effect. Additionally, compounds **6**, **7a** and **8a** displayed moderate $EGFR^{T790M}$ inhibition, with IC_{50} values of 1.00, 0.85 and 0.90

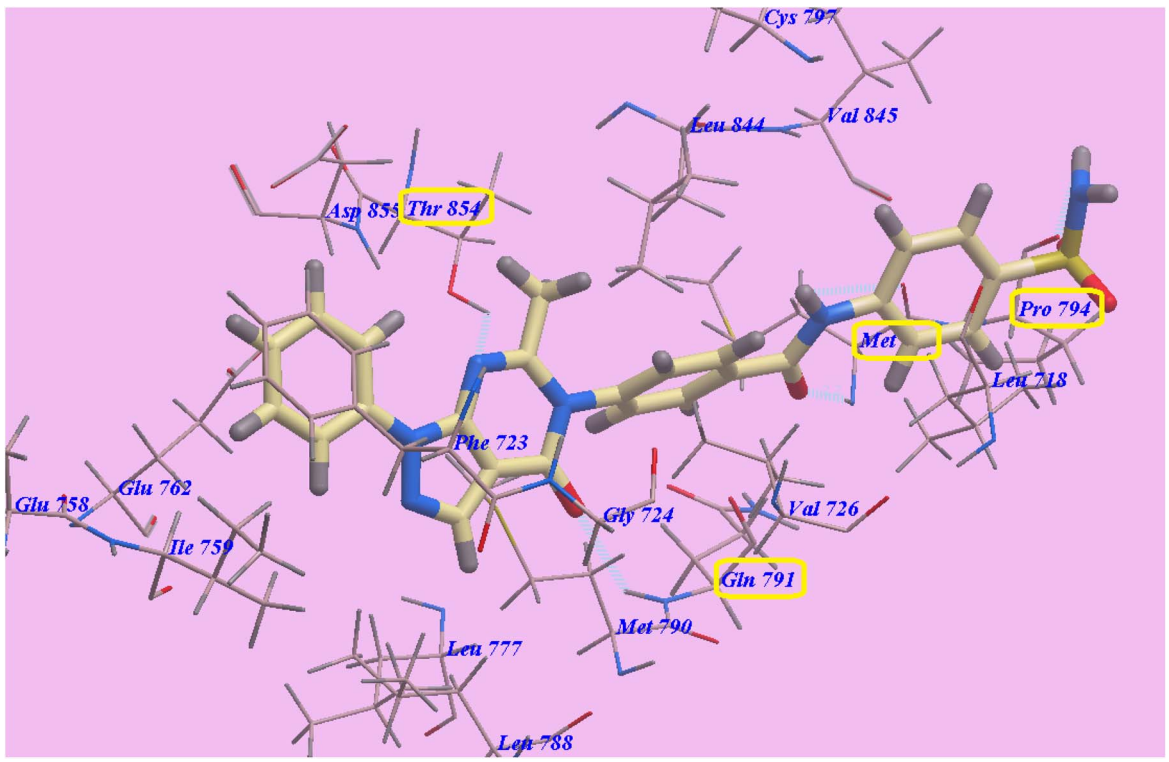

Fig. 10 Predicted binding mode for **7c** with 3W2O.

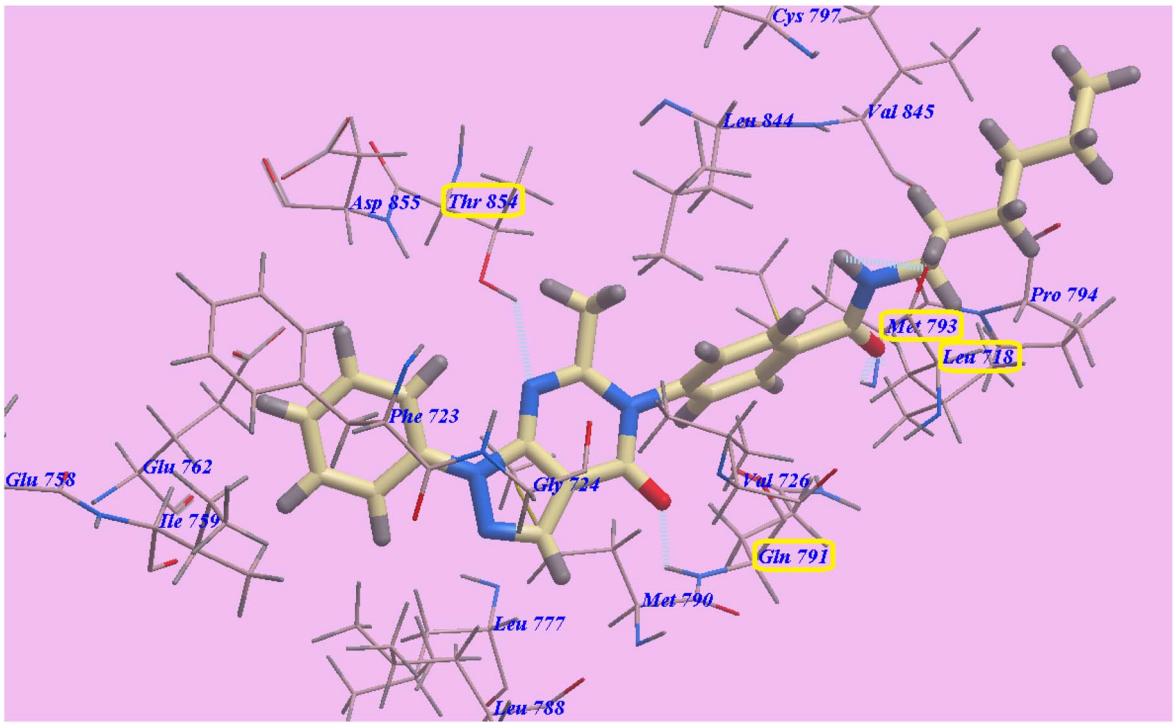

Fig. 11 Docking results for compound **8b** with 3W2O.

μM, respectively. Finally, derivative **5**, with IC_{50} = 1.20 μM, exhibited the lowest $EGFR^{T790M}$ inhibition.

2.6. Structure activity relationship (SAR) studies

The pyrazolopyrimidine rings, linker (HBA-HBD), spacer, lipophilicity, and the electronic nature of the substituents all play an essential role in anticancer activities. Compounds **7c**, **8b**, **7e** and **8c** exhibited the greatest anticancer activities against the four tested cancer cells.

We can classify the tested derivatives into three groups based on their structure (Table 3). The first group contains compounds **5** and **6.** Derivative **6**, with a hydrophobic ethyl ester

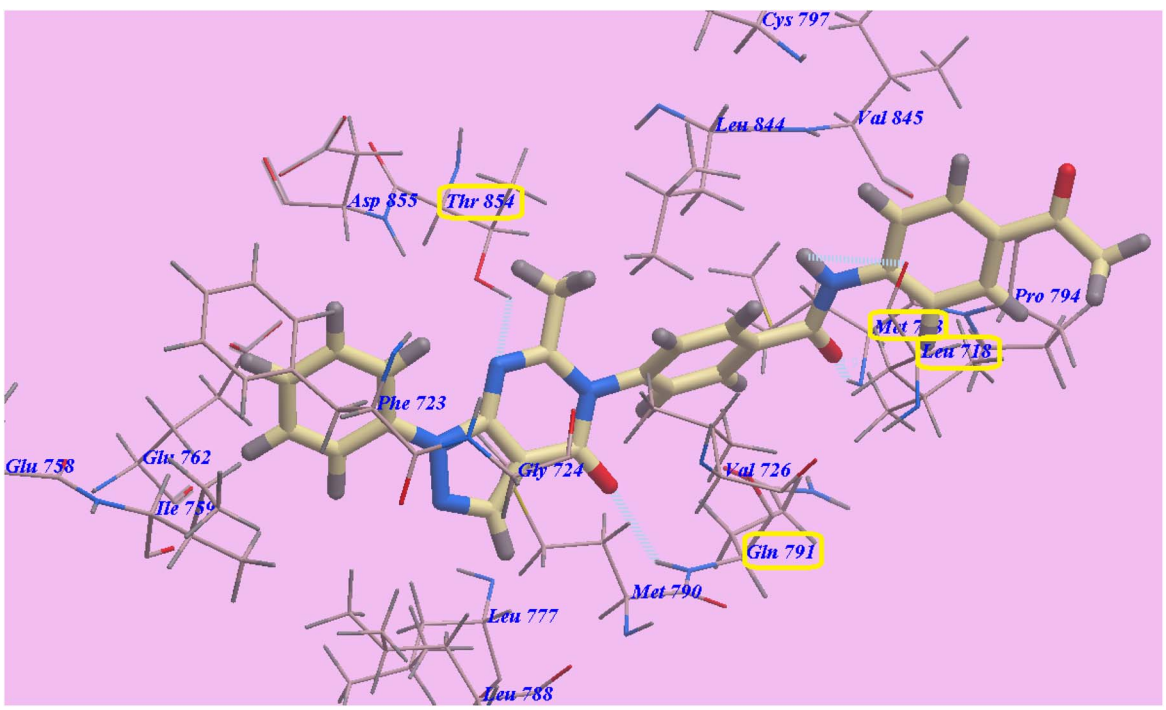

Fig. 12 Docking results for compound **7e** with 3W2O.

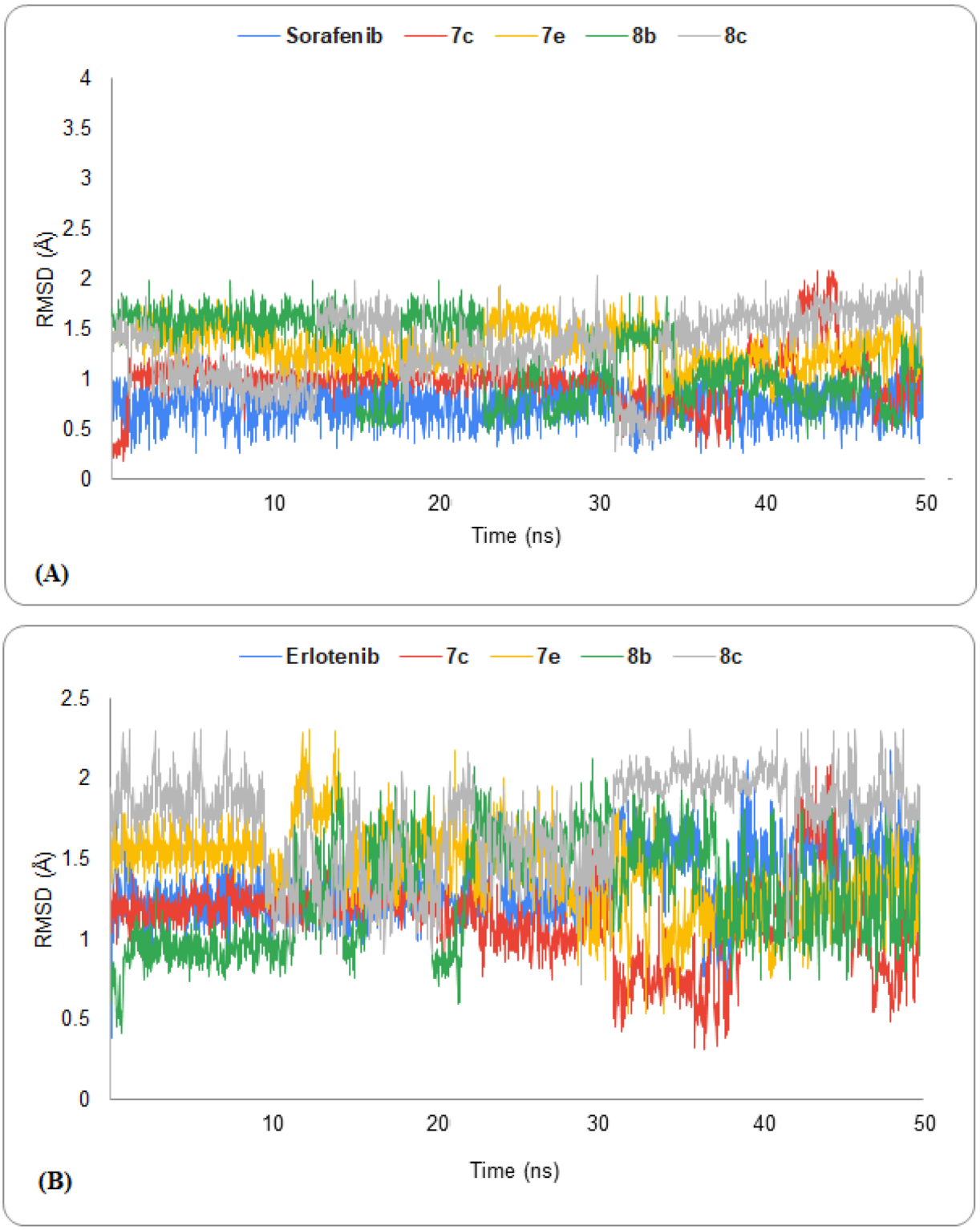

Fig. 13 (A) Analysis of VEGFR-2 protein RMSD throughout 50 ns for the ligand-protein complexes (B) Analysis of $EGFR^{T790M}$ protein RMSD throughout 50 ns for the ligand-protein complexes.

group, showed higher activities against the four cell lines HepG2, MCF-7, A549 and HCT116 than derivative **5**, with an electron-withdrawing hydrophilic COOH group (Fig. 14).

The second group consists of compounds **7a–7e**, all of which contain the *N*-phenyl benzamide moiety. Derivative **7c**, with the phenyl substituted with a hydrophilic electron-withdrawing SO_2NH_2 group, demonstrated higher activities against the four cell lines HepG2, MCF-7, A549, and HCT116 than **7e** (with an electron-withdrawing hydrophobic acetyl group), **7d** (with a hydrophobic electron-donating methoxy group), **7b** (with

Table 3 *In vitro* cytotoxic effects against the HepG2, MCF-7, MCF-10, HCT-116, A549 and VERO cell lines

	IC_{50} (μM)[a]					
Comp.	A549	HCT116	MCF-7	HepG2	MCF-10	VERO
5	17.20 ± 1.5	16.30 ± 1.5	16.10 ± 1.5	16.95 ± 1.5	[b]NT	[b]NT
6	13.00 ± 1.5	12.45 ± 1.5	12.75 ± 1.5	14.70 ± 1.5	[b]NT	[b]NT
7a	10.80 ± 2.5	10.70 ± 1.5	11.15 ± 1.5	12.30 ± 1.5	[b]NT	[b]NT
7b	10.30 ± 1.5	9.50 ± 1.5	10.25 ± 1.5	11.25 ± 1.5	49.95 ± 2.5	47.11 ± 0.50
7c	5.75 ± 1.5	5.50 ± 1.5	5.90 ± 1.5	5.00 ± 1.5	48.80 ± 2.5	47.16 ± 0.50
7d	10.50 ± 1.5	9.40 ± 1.5	10.25 ± 1.5	10.50 ± 1.5	50.55 ± 2.5	52.77 ± 0.50
7e	6.55 ± 1.5	6.15 ± 1.5	7.00 ± 1.5	5.75 ± 1.5	47.45 ± 2.5	44.60 ± 0.50
8a	11.15 ± 1.5	10.25 ± 1.5	10.70 ± 1.5	12.10 ± 1.5	[b]NT	[b]NT
8b	6.20 ± 1.5	5.80 ± 1.5	6.40 ± 1.5	5.30 ± 1.5	56.40 ± 2.5	53.99 ± 0.50
8c	7.10 ± 1.5	7.00 ± 1.5	7.90 ± 1.5	8.80 ± 1.5	39.15 ± 2.5	40.00 ± 0.50
Sorafenib	4.04 ± 0.33	5.58 ± 0.55	5.05 ± 0.50	4.00 ± 0.33	[b]NT	[b]NT
Erlotinib	5.49 ± 0.45	8.20 ± 0.34	13.91 ± 1.3	7.73 ± 0.67	[b]NT	[b]NT

[a] IC_{50} values are the mean ± S.D. of three independent experiments. [b] NT: Not tested compounds.

Table 4 $EGFR^{T790M}$ and VEGFR-2 kinase assays

	IC_{50} (μM)[a]	
Comp	VEGFR-2	$EGFR^{T790M}$
5	2.90 ± 0.50	1.20 ± 0.25
6	2.45 ± 0.50	1.00 ± 0.25
7a	1.70 ± 0.10	0.85 ± 0.25
7b	1.50 ± 0.10	0.45 ± 0.25
7c	0.90 ± 0.50	0.25 ± 0.25
7d	1.95 ± 0.50	0.60 ± 0.25
7e	1.00 ± 0.50	0.35 ± 0.25
8a	2.15 ± 0.50	0.90 ± 0.25
8b	0.95 ± 0.50	0.32 ± 0.25
8c	1.25 ± 0.50	0.50 ± 0.25
Sorafenib	0.84 ± 0.04	[b]NT
Erlotinib	[b]NT	0.24 ± 0.22

[a] IC_{50} values are the mean ± S.D. of three independent experiments. [b] NT: Not tested compounds.

a hydrophilic electron-donating hydroxy group), and the unsubstituted derivative **7a** against the four cell lines, except for A549, for which **7b** > **7d** (Fig. 14).

The third group consists of compounds **8a–8c**, which contain the *N*-alkyl benzamide moiety. Derivative **8b**, with the hydrophobic electron-donating *n*-hexyl group, showed stronger activities against the four cell lines than derivative **8c**, with a hydrophobic electron-donating cyclohexyl group, and **8a**, with a hydrophobic electron-donating ethyl group (Fig. 14).

2.7. ADMET profile and *in silico* studies

The *in silico* ADMET profile analysis of the highly active molecules **7c**, **7e** and **8b** was performed using the pkCSM descriptor[63] and related to Lipinski's rule of five.[64] Good absorption characteristics were expected for compounds with at least three rules: (i) HBD ≤5, (ii) log P ≤5, (iii) molecular weight <500, (iv) and HBA ≤10. The standard anticancer agent sorafenib and compound **7c** break one rule, while compounds **7e** and **8b**, as well as erlotinib, do not break any of the rules (Table 5).

Our derivatives have excellent GIT absorption in humans (86.8–100.0), which indicates that they can penetrate different cellular membranes easily.[65] As a result, they may exhibit significantly high bioavailability across the GIT. Our products are capable of penetrating the CNS (CNS permeability = −2.043–3.188), with CNS permeabilities lower than that of sorafenib (CNS permeability = −2.007) but greater than that of erlotinib (CNS permeability = −3.216).

Sorafenib, erlotinib, **7e** and **8b** may inhibit metabolism through inhibition of CYP3A4. Moreover, sorafenib, **7c** and **7e** showed poor clearance values. Erlotinib and **8b** exhibited greater clearance rates. As a result, erlotinib and **8b** have shorter dose intervals, since they can be eliminated from the body more rapidly. Derivatives **7c** and **7e**, in contrast to erlotinib, exhibited slow clearance rates, which suggests a longer half-life and prolonged dose intervals. Sorafenib, erlotinib, and the new molecules all had unfavorable hepatotoxicity. The three derivatives **7c**, **7e** and **8b** showed maximum tolerated doses higher than that of sorafenib but lower than that of erlotinib. Finally, the novel derivatives showed acute toxic doses higher than those of both sorafenib and erlotinib.

3. Experimental

3.1. Chemistry

3.1.1. General. According to the described processes,[48,49] the starting and intermediate products ethyl 2-cyano-3-ethoxyacrylate (**1**), ethyl 5-amino-1-phenyl-1*H*-pyrazole-4-carboxylate (**2**), 5-amino-1-phenyl-1*H*-pyrazole-4-carboxylate (**3**), and 6-methyl-1-phenylpyrazolo[3,4-*d*][1,3]oxazin-4(1*H*)-one (**4**) were synthesized. Each compound was obtained by crystallization from ethanol, and the NMR spectra were recorded at 400 MHz for ^{1}H NMR and 100 MHz for ^{13}C NMR in DMSO-d_6.

3.1.2. General procedure for the syntheses of compounds 5 and 6. 6-Methyl-1-phenylpyrazolo[3,4-*d*][1,3]oxazin-4(1*H*)-one (**4**) (2.27 g, 0.01 mol) was refluxed for 6 hours with an equimolar amount of either 4-aminobenzoic acid or ethyl 4-aminobenzoate (0.01 mol). The mixture was allowed to reach room

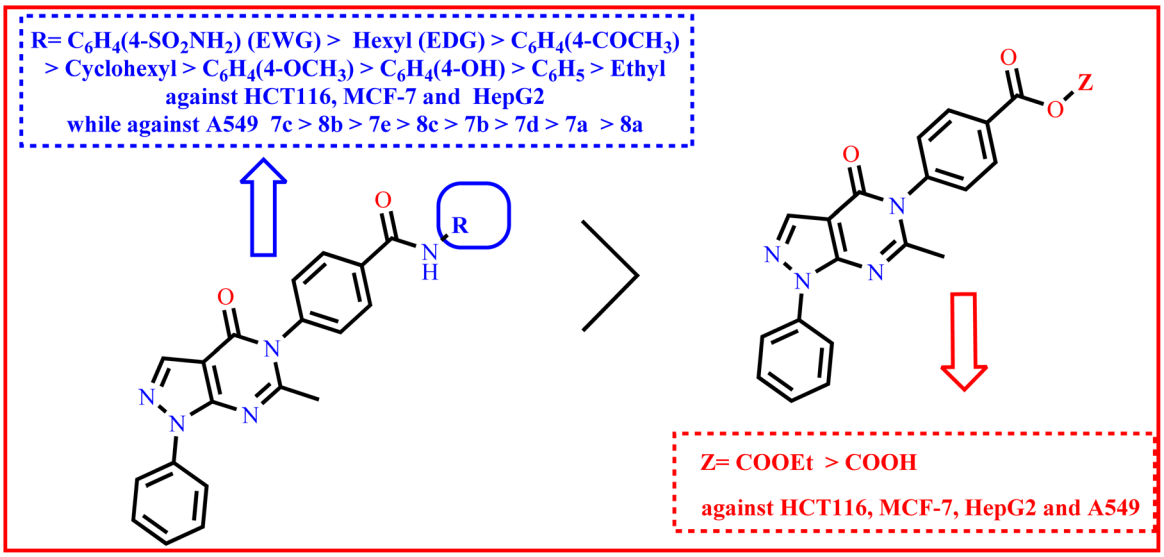

Fig. 14 Schematic for the SAR study.

temperature, then poured on an ice-water mixture to separate the solids, which were then filtered and crystallized from ethanol to obtain the desired compounds **5** and **6**, respectively.

3.1.2.1. 4-(6-Methyl-4-oxo-1-phenyl-1,4-dihydro-5H-pyrazolo [3,4-d]pyrimidin-5-yl)benzoic acid (5). Yield 85%; m.p. 237–9 °C; $IR_{\nu_{max}}$ (cm^{-1}): 3421 (OH), 3050 (CH aromatic), 2964 (CH aliphatic), 1713, 1631 (2C=O); ^1H NMR (400 MHz, DMSO-d_6): 2.18 (s, 3H, CH_3), 7.42–7.45 (m, H, H-4 of C_6H_5), 7.52–7.64 (m, 4H, H-3, H-5 of C_6H_4 and H-3, H-5 of C_6H_5), 8.09–8.15 (m, 4H, H-2, H-6 of C_6H_4 and H-2, H-6 of C_6H_5), 8.37 (s, 1H, CH of pyrazole), 12.62 (s, 1H, OH, D_2O exchangeable); ^{13}C NMR (100 MHz, DMSO-d_6): 26.68, 110.95, 121.76 (2), 122.30 (2), 126.61, 129.15 (2), 129.40, 130.51 (2), 137.86, 140.92, 142.68, 143.86, 150.19, 165.79, 167.19; Anal. Calcd. For $C_{19}H_{14}N_4O_3$ (m.w.

Table 5 ADMET profiles of the most effective compounds **7c**, **7e**, **8b**, sorafenib and erlotinib

Parameter	7c	7e	8b	Sorafenib	Erlotinib
Physicochemical properties					
Molecular weight (Daltons)	500.54	463.497	429.524	464.831	393.443
LogP	2.77952	4.33472	3.18992	5.5497	3.4051
Rotatable bonds	5	5	8	5	10
Acceptors	8	7	6	4	7
Donors	2	1	1	3	1
Surface area (Å^2)	205.244	200.035	186.276	185.111	169.532
Absorption					
Human intestinal absorption (%)	86.799	100.000	98.092	89.043	94.58
Distribution					
BBB permeability (log BB)	−1.158	−0.741	−0.855	−1.684	−0.745
CNS permeability (log PS)	−3.188	−2.043	−2.325	−2.007	−3.216
Metabolism					
Inhibition of CYP3A4	No	Yes	Yes	Yes	Yes
Inhibition of CYP2D6	No	No	No	Yes	Yes
Inhibition of CYP1A2	No	Yes	Yes	Yes	Yes
Inhibition of CYP2C19	Yes	Yes	Yes	No	No
Inhibition of CYP2C9	Yes	Yes	Yes	Yes	Yes
Excretion					
Clearance (log mL^{-1} min kg^{-1})	0.531	0.31	0.711	−0.219	0.702
Toxicity					
Human max. Tolerated dose (log mg^{-1} kg per day)	0.661	0.678	0.601	0.549	0.839
Acute toxic activity (LD_{50}) (mol kg^{-1})	3.168	2.97	2.816	2.538	2.393
Hepatotoxic effect	Yes	Yes	Yes	Yes	Yes

346.35): C, 65.89; H, 4.07; N, 16.18. Found: C, 65.80; H, 4.00; N, 16.05.

*3.1.2.2. Ethyl 4-(6-methyl-4-oxo-1-phenyl-1,4-dihydro-5H-pyrazolo[3,4-d]pyrimidin-5-yl)benzoate (**6**).* Yield 80%; m.p. 180–2 °C; $IR_{\nu_{max}}$ (cm^{-1}): 3085 (CH aromatic), 2979 (CH aliphatic), 1725, 1658 (2C=O); ^1H NMR (400 MHz, DMSO-d_6): 1.34–1.37 (t, 3H, CH_2CH_3), 2.18 (s, 3H, CH_3), 4.35–4.40 (q, 2H, CH_2CH_3), 7.41–7.45 (m, H, H-4 of C_6H_5), 7.58–7.64 (m, 4H, H-3, H-5 of C_6H_4 and H-3, H-5 of C_6H_5), 8.09–8.16 (m, 4H, H-2, H-6 of C_6H_4 and H-2, H-6 of C_6H_5), 8.37 (s, 1H, CH of pyrazole); ^{13}C NMR (100 MHz, DMSO-d_6): 14.57, 25.02, 61.64, 105.75, 120.71 (2), 122.29, 126.99, 127.73 (2), 129.62 (2), 130.95 (2), 136.77, 138.59, 142.19, 151.18, 157.94, 158.97, 165.62; Anal. Calcd. For $C_{21}H_{18}N_4O_3$ (m.w. 374.14): C, 67.37; H, 4.85; N, 14.96. Found: C, 67.50; H, 4.95; N, 14.85.

3.1.3. General procedure for synthesis of compounds 7a–e. Et_3N (0.1 g, 0.2 mL, 0.001 mol) was added to a suspension of 4-(6-methyl-4-oxo-1-phenyl-1,4-dihydro-5*H*-pyrazolo[3,4-*d*] pyrimidin-5-yl)benzoic acid (**5**) (0.35 g, 0.001 mol) in DCM (10 mL). The reaction mixture was stirred in an ice-salt bath for 10 min. To the clear solution, ethyl chloroformate (0.11 g, 0.1 mL, 0.001 mol) was added in a dropwise manner over a period of 20 min, and the reaction mixture was stirred for 1 h in the ice-salt bath. Then, a solution of the appropriate aromatic amine (0.001 mol), namely, aniline, 4-aminophenol, 4-aminobenzenesulfonamide, 4-methoxyaniline and/or 4-aminoacetophenone and TEA (0.1 g, 0.2 mL, 0.001 mol) in DCM (10 mL) was added to the previous mixture. The whole mixture was stirred overnight at r.t. and the obtained precipitate was filtered, washed with water followed by hot ethanol, and dried to provide the corresponding amide derivatives **7a–e**, respectively.

*3.1.3.1. 4-(6-Methyl-4-oxo-1-phenyl-1,4-dihydro-5H-pyrazolo[3,4-d]pyrimidin-5-yl)-N-phenylbenzamide (**7a**).* Yield 87%; m.p. 202–4 °C; $IR_{\nu_{max}}$ (cm^{-1}): 3318 (NH), 3068 (CH aromatic), 2979 (CH aliphatic), 1695, 1641 (2C=O); ^1H NMR (400 MHz, DMSO-d_6): 2.24 (s, 3H, CH_3), 7.12–7.16 (m, H, H-4 of NHC_6H_5), 7.35–7.47 (m, 2H, H-3, H-5 of NHC_6H_5), 7.55–7.57 (m, 2H, H-2, H-6 of C_6H_4), 7.61–7.66 (m, H, H-4 C_6H_5), 7.79–7.83 (m, 2H, H-3, H-5 of C_6H_5), 7.88–7.91 (m, 2H, H-2, H-6 of NHC_6H_5), 7.99–8.01 (m, 2H, H-3, H-5 of C_6H_4), 8.12–8.14 (m, 2H, H-2, H-6 of C_6H_4), 8.42 (s, 1H, CH of pyrazole), 10.15 (s, 1H, NH, D_2O exchangeable); ^{13}C NMR (100 MHz, DMSO-d_6): 21.55, 108.50, 110.06, 115.83 (2), 118.39 (2), 119.06 (2), 121.26 (2), 122.39 (2), 128.97, 129.31, 130.62, 131.75, 138.78 (2), 147.97, 148.08, 149.08, 152.75, 153.11, 153.73; Anal. Calcd. For $C_{25}H_{19}N_5O_2$ (m.w. 421.15): C, 71.25; H, 4.54; N, 16.62; O, 7.59. Found: C, 71.20; H, 4.54; N, 16.75; O, 7.70.

*3.1.3.2. N-(4-Hydroxyphenyl)-4-(6-methyl-4-oxo-1-phenyl-1,4-dihydro-5H-pyrazolo[3,4-d]pyrimidin-5-yl)benzamide (**7b**).* Yield 78%; m.p. 205–7 °C; $IR_{\nu_{max}}$ (cm^{-1}): 3439 (OH), 3315 (NH), 3075 (CH aromatic), 2950 (CH aliphatic), 1711, 1695 (2C=O); ^1H NMR (400 MHz, DMSO-d_6): 2.18 (s, 3H, CH_3), 7.38–7.48 (m, 2H, H-3, H-5 of NHC_6H_5), 7.55–7.61 (m, 3H, H-2, H-6 of NHC_6H_4 and H-4 C_6H_5), 7.66–7.68 (m, 2H, H-2, H-6 of C_6H_4), 7.72–7.77 (m, 2H, H-3, H-5 of C_6H_5), 8.01–8.02 (m, 2H, H-3, H-5 of C_6H_4), 8.08–8.10 (m, 2H, H-2, H-6 of C_6H_5), 8.35 (s, 1H, CH of pyrazole), 10.33 (s, 1H, NH, D_2O exchangeable), 12.09 (s, 1H, OH, D_2O exchangeable); ^{13}C NMR (100 MHz, DMSO-d_6): 26.74, 106.07 (2), 106.53, 117.11 (2), 118.95 (2), 120.14 (2), 121.95, 128.57 (2), 129.34 (2), 130.97, 139.96, 142.87, 143.90, 145.01 (2), 150.18, 154.38, 165.12, 167.20; Anal. Calcd. For $C_{25}H_{19}N_5O_3$ (m.w. 437.15): C, 68.64; H, 4.38; N, 16.01. Found: C, 68.55; H, 4.45; N, 15.95.

*3.1.3.3. 4-(6-Methyl-4-oxo-1-phenyl-1,4-dihydro-5H-pyrazolo[3,4-d]pyrimidin-5-yl)-N-(4-sulfamoylphenyl)-benzamide (**7c**).* Yield 83%; m.p. 232–4 °C; $IR_{\nu_{max}}$ (cm^{-1}): 3310, 3240 (NH_2 and NH), 3066 (CH aromatic), 2986 (CH aliphatic), 1715, 1699 (2C=O); ^1H NMR (400 MHz, DMSO-d_6): 2.23 (s, 3H, CH_3), 6.88 (s, 2H, NH_2, D_2O exchangeable), 7.27–7.45 (m, 2H, H-2, H-6 of C_6H_4), 7.58–7.67 (m, 5H, H-3, H-4, H-5 of C_6H_5 and H-3, H-5 of $C_6H_4SO_2NH_2$), 7.75–7.98 (m, 2H, H-3, H-5 of C_6H_4), 8.09–8.15 (m, 4H, H-2, H-6 of C_6H_5 and H-2, H-6 of $C_6H_4SO_2NH_2$), 8.38 (s, 1H, CH of pyrazole), 10.42 (s, 1H, NH, D_2O exchangeable); ^{13}C NMR (100 MHz, DMSO-d_6): 21.53, 108.47, 109.27, 113.34, 115.77, 116.83 (2), 117.30 (2), 119.96 (2), 121.66 (2), 122.80 (2), 127.58, 129.09 (2), 130.70, 138.79, 139.02, 147.93, 149.19, 152.70, 153.69; Anal. Calcd. For $C_{25}H_{20}N_6O_4S$ (m.w. 500.13): C, 59.99; H, 4.03; N, 16.79. Found: C, 60.12; H, 4.10; N, 16.88.

*3.1.3.4. N-(4-Methoxyphenyl)-4-(6-methyl-4-oxo-1-phenyl-1,4-dihydro-5H-pyrazolo[3,4-d]pyrimidin-5-yl)benzamide (**7d**).* Yield 86%; m.p. 200–2 °C; $IR_{\nu_{max}}$ (cm^{-1}): 3402 (NH), 3068 (CH aromatic), 2930 (CH aliphatic), 1711, 1654 (2C=O); ^1H NMR (400 MHz, DMSO-d_6): 2.18 (s, 3H, CH_3), 3.76 (s, 3H, OCH_3), 6.84–6.97 (m, 2H, H-3, H-5 of $C_6H_5OCH_3$), 7.33–7.46 (m, 2H, H-2, H-6 of C_6H_4), 7.59–7.72 (m, 5H, H-3, H-4, H-5 of C_6H_5 and H-2, H-6 of $C_6H_5OCH_3$), 8.09–8.16 (m, 4H, H-3, H-5 of C_6H_4 and H-2, H-6 of C_6H_5), 8.38 (s, 1H, CH of pyrazole), 10.30 (s, 1H, NH, D_2O exchangeable); ^{13}C NMR (100 MHz, DMSO-d_6): 25.09, 61.57, 105.85, 122.19 (4), 127.65, 129.69 (4), 129.80 (2), 130.92 (2), 131.08 (2), 136.84 (2), 138.70, 142.29, 151.21, 157.84, 158.95, 165.55; Anal. Calcd. For $C_{26}H_{21}N_5O_3$ (m.w. 451.16): C, 69.17; H, 4.69; N, 15.51. Found: C, 69.25; H, 4.75; N, 15.50.

*3.1.3.5. N-(4-Acetylphenyl)-4-(6-methyl-4-oxo-1-phenyl-1,4-dihydro-5H-pyrazolo[3,4-d]pyrimidin-5-yl)benzamide (**7e**).* Yield 84%; m.p. 220–2 °C; $IR_{\nu_{max}}$ (cm^{-1}): 3316 (NH), 3064 (CH aromatic), 2985 (CH aliphatic), 1716, 1698, 1668 (3C=O); ^1H NMR (400 MHz, DMSO-d_6): 2.22 (s, 3H, CH_3), 2.57 (s, 3H, $COCH_3$), 7.42–7.46 (m, H, H-4 of C_6H_5), 7.59–7.67 (m, 4H, H-2, H-6 of C_6H_4 and H-3, H-5 of C_6H_5), 7.96–8.02 (m, 4H, H-3, H-5 of C_6H_4 and H-2, H-6 of $C_6H_5COCH_3$), 8.09–8.16 (m, 4H, H-2, H-6 of C_6H_5 & H-3, H-5 of $C_6H_5COCH_3$), 8.39 (s, 1H, CH of pyrazole), 10.73 (s, 1H, NH, D_2O exchangeable); ^{13}C NMR (100 MHz, DMSO-d_6): 21.58, 23.78, 106.05, 108.53, 114.60 (2), 115.68, 118.34 (2), 121.30 (2), 127.73 (2), 129.35 (2), 130.82, 138.43 (2), 144.19, 147.65, 152.91, 153.77, 154.03, 155.32, 163.64, 172.34, 174.55; MS (*m*/*z*): 463.03 (M^+, 27.20%), 445.57 (70.52%), 363.49 (71.93%), 318.85 (70.56%), 183.37 (100%, base beak); Anal. Calcd. For $C_{27}H_{21}N_5O_3$ (m.w. 463.16): C, 69.97; H, 4.57; N, 15.11. Found: C, 70.10; H, 4.66; N, 15.00.

3.1.4. General procedure for synthesis of compounds 8a–c. TEA (0.1 g, 0.2 mL, 0.001 mol) was added to a suspension of 4-(6-methyl-4-oxo-1-phenyl-1,4-dihydro-5*H*-pyrazolo[3,4-*d*] pyrimidin-5-yl)benzoic acid (**5**) (0.35 g, 0.001 mol) in DCM (10

mL). The reaction mixture was stirred in an ice-salt bath for 10 min. To the clear solution, ethyl chloroformate (0.11 g, 0.1 mL, 0.001 mol) was added in a dropwise manner over a period of 20 min, and the reaction mixture was stirred for 1 h in the ice-salt bath. Then, a solution of the appropriate aliphatic amine (0.001 mol), namely, ethylamine, *n*-hexylamine and/or cyclohexylamine and TEA (0.1 g, 0.2 mL, 0.001 mol) in DCM (10 mL) was added to the previous mixture. The whole mixture was stirred overnight at r.t., and the obtained precipitate was filtered, washed with water followed by hot ethanol, and dried to provide the corresponding amide derivatives **8a–c**, respectively.

*3.1.4.1. N-Ethyl-4-(6-methyl-4-oxo-1-phenyl-1,4-dihydro-5H-pyrazolo[3,4-d]pyrimidin-5-yl)benzamide (**8a**).* Yield 83%; m.p. 210–2 °C; $IR_{\nu_{max}}$ (cm^{-1}): 3400 (NH), 3066 (CH aromatic), 2981 (CH aliphatic), 1714 (2C=O); ^1H NMR (400 MHz, DMSO-d_6): 1.18 (t, 3H, CH_2CH_3), 2.18 (s, 3H, CH_3), 3.30–3.35 (q, 2H, CH_2CH_3), 7.41–7.44 (m, H, H-4 of C_6H_5), 7.52–7.64 (m, 4H, H-2, H-6 of C_6H_4CO and H-3, H-5 of C_6H_5), 8.00–8.03 (m, 2H, H-3, H-5 of C_6H_4CO), 8.09–8.15 (m, 2H, H-2, H-6 of C_6H_5), 8.36 (s, 1H, CH of pyrazole), 8.64 (s, 1H, NH, D_2O exchangeable); ^{13}C NMR (100 MHz, DMSO-d_6): 14.62, 25.12, 34.63, 105.88, 122.15 (2), 127.60 (2), 128.93 (2), 129.78 (2), 135.87, 136.82, 138.73, 140.30, 142.35, 144.53, 157.89, 158.93, 165.70; MS (*m*/*z*): 373.21 (M^+, 15.17%), 343.47 (88.40%), 264.30 (53.38%), 180.37 (100%, base beak); Anal. Calcd. For $C_{21}H_{19}N_5O_2$ (m.w. 373.15): C, 67.55; H, 5.13; N, 18.76. Found: C, 67.48; H, 4.98; N, 18.69.

*3.1.4.2. N-Hexyl-4-(6-methyl-4-oxo-1-phenyl-1,4-dihydro-5H-pyrazolo[3,4-d]pyrimidin-5-yl)benzamide (**8b**).* Yield 81%; m.p. 233–5 °C; $IR_{\nu_{max}}$ (cm^{-1}): 3308 (NH), 3066 (CH aromatic), 2986 (CH aliphatic), 1714, 1649 (2C=O); ^1H NMR (400 MHz, DMSO-d_6): 1.14–1.22 (t, 3H, CH_2CH_3), 1.31–1.38 (m, 4H, CH_2CH_2), 1.75–1.85 (m, 4H, CH_2CH_2), 2.18 (s, 3H, CH_3), 3.05–3.09 (t, 2H, $NHCH_2CH_2$), 7.43–7.45 (m, H, H-4 of C_6H_5), 7.52–7.64 (m, 4H, H-2, H-6 of C_6H_4 and H-3, H-5 of C_6H_5), 8.00–8.03 (m, 2H, H-3, H-5 of C_6H_4), 8.09–8.11 (m, 2H, H-2, H-6 of C_6H_5), 8.37 (s, 1H, CH of pyrazole), 9.15 (s, 1H, NH, D_2O exchangeable); ^{13}C NMR (100 MHz, DMSO-d_6): 14.56, 19.06, 22.04, 24.42, 28.06, 31.61, 36.73, 110.95, 121.77 (2), 122.23 (2), 126.42, 126.83, 128.43, 129.08 (2), 129.66 (2), 136.33, 140.24, 142.16, 150.20, 165.46, 167.06; Anal. Calcd. For $C_{25}H_{27}N_5O_2$ (m.w. 429.22): C, 69.91; H, 6.34; N, 16.31. Found: C, 70.00; H, 6.30; N, 16.25.

*3.1.4.3. N-Cyclohexyl-4-(6-methyl-4-oxo-1-phenyl-1,4-dihydro-5H-pyrazolo[3,4-d]pyrimidin-5-yl)benzamide (**8c**).* Yield 77%; m.p. 217–9 °C; $IR_{\nu_{max}}$ (cm^{-1}): 3227 (NH), 3077 (CH aromatic), 2930 (CH aliphatic), 1715, 1633 (2C=O); ^1H NMR (400 MHz, DMSO-d_6): 1.10–1.20 (m, 2H, CH_2), 1.30–1.40 (m, 4H, CH_2CH_2), 1.62–1.85 (m, 4H, CH_2CH_2), 2.19 (s, 3H, CH_3), 3.79 (m, H, NHCH), 7.42–7.45 (m, 2H, H-2, H-6 of C_6H_4), 7.53–7.55 (m, H, H-4 of C_6H_5), 7.58–7.64 (m, 3H, H-3, H-5 of C_6H_5 and NH, D_2O exchangeable), 7.99–8.16 (m, 4H, H-3, H-5 of C_6H_4 and H-2, H-6 of C_6H_5), 8.37 (s, 1H, CH of pyrazole); ^{13}C NMR (100 MHz, DMSO-d_6): 14.61, 25.09 (2), 25.37, 32.84 (2), 61.57, 105.85, 122.17 (2), 127.62, 128.91 (2), 129.10 (2), 129.79, 130.92, 135.94, 136.83 (2), 138.70, 151.20, 157.93, 158.95, 165.15; MS (*m*/*z*): 427.34 (M^+, 19.19%), 395.49 (100%, base beak), 371.64 (44.64%), 281.49 (74.54%), 95.60 (86.91%), 57.12 (74.21%), 43.01 (66.11%); Anal. Calcd. For $C_{25}H_{25}N_5O_2$ (m.w. 427.20): C, 70.24; H, 5.89; N, 16.38. Found: C, 70.30; H, 5.95; N, 16.25.

4. Conclusion

In conclusion, the newly designed pyrazolo[3,4-*d*]pyrimidine derivatives were synthesized and tested against HepG2, A549, MCF-7 and HCT-116 as dual VEGFR-2 and $EGFR^{T790M}$ inhibitors. The proposed mode of their interactions with VEGFR-2 and $EGFR^{T790M}$ was investigated using molecular design. The data from the docking studies and the results of the biological screening were excellently correlated. In general, derivatives **7c**, **8b**, **7e** and **8c** exhibited very good anticancer effects, with IC_{50} values of 5.75, 6.20, 6.55 and 7.10 μM, respectively, against A549. Derivatives **6**, **7a**, **7b**, **7d** and **8a**, with IC_{50} values of 10.30–13.00 μM, showed good cytotoxicity. Against HCT-116, derivatives **7c**, **8b**, **7e**, **8c**, **7d** and **7b**, with IC_{50} values of 5.50, 5.80, 6.15, 7.00, 9.40 and 9.50 μM, respectively, exhibited very good anticancer effects. Derivatives **6**, **7a** and **8a**, with IC_{50} values of 12.45, 10.70, and 10.25 μM, respectively, showed good cytotoxicity. Concerning MCF-7, derivatives **7c**, **8b**, **7e** and **8c** exhibited very good anticancer effects with IC_{50} values of 5.90, 6.40, 7.00 and 7.90 μM, respectively. Derivatives **6**, **7a**, **7b**, **7d** and **8a**, with IC_{50} values of 10.25–12.75 μM, showed good cytotoxicity. Regarding HepG2, derivatives **7c**, **8b**, **7e** and **8c**, with IC_{50} values of 5.00, 5.30, 5.75 and 8.80 μM, respectively, exhibited very good anticancer effects. Derivatives **6**, **7a**, **7b**, **7d** and **8a** showed good cytotoxicity, with IC_{50} values of 10.50–14.70 μM. Moreover, the six extremely viable structures **7b**, **7c**, **7d**, **7e**, **8b** and **8c** were tested against VERO normal cell lines to estimate their cytotoxic capabilities. All the results confirm that each of the compounds exhibit poor toxicity toward normal VERO cells, with IC_{50} values ranging from 40.00 to 53.99 μM. Furthermore, all the derivatives **5–8a–c** were tested as VEGFR-2 and $EGFR^{T790M}$ inhibitors. The most active derivatives, which showed very good inhibition against VEGFR-2, were found to be derivatives **7c**, **8b**, **7e** and **8c**, with IC_{50} values of 0.90 to 1.25 μM. The IC_{50} for compounds **7a**, **7b** and **7d** were 1.50–1.95 μM and showed good activity. In addition, derivatives **7c**, **8b**, **7e**, **7b** and **8c**, with IC_{50} values of 0.25, 0.32, 0.35, 0.45 and 0.50 μM, respectively, showed very good $EGFR^{T790M}$ inhibition. Furthermore, compound **7d**, with IC_{50} = 0.60 μM, showed good inhibition activity. The ADMET profiles for the three most active compounds **7c**, **7e** and **8b**, were computed *in silico*, using sorafenib and erlotinib as reference medicines, and they presented excellent ADMET profiles.

Conflicts of interest

The authors declare no conflicts of interest.

Data availability

The data supporting this article are available upon request.

Supplementary information (SI) is available. See DOI: https://doi.org/10.1039/d6ra00037a.

References

1 M. A. Abdelgawad, N. A. A. Elkanzi, A. A. Nayl, A. Musa, N. H. Alotaibi, W. A. A. Arafa, S. M. Gomha and R. B. Bakr, Targeting tumor cells with pyrazolo[3,4-*d*]pyrimidine scaffold: A literature review on synthetic approaches, structure activity relationship, structural and target-based mechanisms, *Arab. J. Chem.*, 2022, **15**(5), 103781, DOI: 10.1016/j.arabjc.2022.103781.

2 J. Fares, M. Y. Fares, H. H. Khachfe, H. A. Salhab and Y. Fares, Molecular principles of metastasis: a hallmark of cancer revisited, *Signal Transduct. Targeted Ther.*, 2020, **5**, 1–17.

3 G. Follain, D. Herrmann, S. Harlepp, V. Hyenne, N. Osmani, S. C. Warren, P. Timpson and J. G. Goetz, Fluids and their mechanics in tumour transit: shaping metastasis, *Nat. Rev. Cancer*, 2020, **20**, 107–124.

4 T. B. Steinbichler, D. Savic, J. Dudaá, I. Kvitsaridze, S. Skvortsov, H. Riechelmann and I.-I. Skvortsova, Cancer stem cells and their unique role in metastatic spread, *Semin. Cancer Biol.*, 2020, 148–156.

5 D. Alferez, R. W. Wilkinson, J. Watkins, R. Poulsom, N. Mandir, S. R. Wedge, I. T. Pyrah, N. R. Smith, L. Jackson, A. J. Ryan and R. A. Goodlad, Dual inhibition of VEGFR and EGFR signaling reduces the incidence and size of intestinal adenomas in Apc(Min/+) mice, *Mol. Cancer Ther.*, 2008, **7**(3), 590–598.

6 A. E. Mghwary, E. M. Gedawy, A. M. Kamal and S. M. Abuel-Maaty, Novel thienopyrimidine derivatives as dual EGFR and VEGFR-2 inhibitors: design, synthesis, anticancer activity and effect on cell cycle profile, *J. Enzyme Inhib. Med. Chem.*, 2019, **34**, 838–852, DOI: 10.1080/14756366.2019.1593160.

7 S. A. Lang, P. Schachtschneider, C. Moser, A. Mori, C. Hackl, A. Gaumann, D. Batt, H. J. Schlitt, E. K. Geissler and O. Stoeltzing, Dual targeting of Raf and VEGF receptor 2 reduces growth and metastasis of pancreatic cancer through direct effects on tumor cells, endothelial cells, and pericytes, *Mol. Cancer Ther.*, 2008, **7**, 3509–3518, DOI: 10.1158/1535-7163.MCT-08-0373.

8 A. K. Larsen, D. Ouaret, K. El Ouadrani and A. Petitprez, Targeting EGFR and VEGF(R) pathway cross-talk in tumor survival and angiogenesis, *Pharmacol. Ther.*, 2011, **131**, 80–90.

9 P. A. Jänne, J. C. Yang, D. W. Kim, D. Planchard, Y. Ohe, S. S. Ramalingam, M. J. Ahn, S. W. Kim, W. C. Su, L. Horn, D. Haggstrom, E. Felip, J. H. Kim, P. Frewer, M. Cantarini, K. H. Brown, P. A. Dickinson, S. Ghiorghiu and M. Ranson, AZD9291 in EGFR inhibitor-resistant non-small-cell lung cancer, *N. Engl. J. Med.*, 2015, **372**, 1689–1699.

10 X. Le, M. Nilsson, J. Goldman, M. Reck, K. Nakagawa, T. Kato, L. P. Ares, B. Frimodt-Moller, K. Wolff, C. Visseren-Grul, J. V. Heymach and E. B. Garon, Dual EGFR-VEGF Pathway Inhibition: A Promising Strategy for Patients With EGFR-Mutant NSCLC, *J. Thorac. Oncol.*, 2021, **16**(2), 205–215, DOI: 10.1016/j.jtho.2020.10.006.

11 L. Xi, J. Q. Zhang, Z. C. Liu, J. H. Zhang, J. F. Yan, Y. Jin and J. Lin, Novel 5-anilinoquinazoline-8-nitro derivatives as inhibitors of VEGFR-2 tyrosine kinase: synthesis, biological evaluation and molecular docking, *Org. Biomol. Chem.*, 2013, **11**, 4367–4378, DOI: 10.1039/c3ob40368h.

12 N. M. Saleh, M. G. El-Gazzar, H. M. Aly and R. A. Othman, Novel Anticancer Fused Pyrazole Derivatives as EGFR and VEGFR-2 Dual TK Inhibitors, *Front. Chem.*, 2020, **7**, 917, DOI: 10.3389/fchem.2019.00917.

13 N. Berndt, R. M. Karim and E. Schonbrunn, Advances of small molecule targeting of kinases, *Curr. Opin. Chem. Biol.*, 2017, **39**, 126–132, DOI: 10.1016/j.cbpa.2017.06.015.

14 M. E. Breen and M. B. Soellner, Small molecule substrate phosphorylation site inhibitors of protein kinases: approaches and challenges, *ACS Chem. Biol.*, 2015, **10**, 175–189, DOI: 10.1021/cb5008376.

15 D. Fabbro, 25 years of small molecular weight kinase inhibitors: potentials and limitations, *Mol. Pharmacol.*, 2015, **87**, 766–775, DOI: 10.1124/mol.114.095489.

16 P. M. Fischer, Approved and experimental small-molecule oncology kinase inhibitor drugs: a mid-2016 overview, *Med. Res. Rev.*, 2017, **37**, 314–367, DOI: 10.1002/med.21409.

17 X. Li, Z. Li, X. Wu, Z. Xiong, T. Yang, Z. Fu, X. Liu, X. Tan, F. Zhong and X. Wan, Deep learning enhancing kinome-wide polypharmacology profiling: model construction and experiment validation, *J. Med. Chem.*, 2019, **63**, 8723–8737.

18 O. A. Hamed, N. Abou-Elmagd El-Sayed, W. R. Mahmoud and G. F. Elmasry, Molecular docking approach for the design and synthesis of new pyrazolopyrimidine analogs of roscovitine as potential CDK2 inhibitors endowed with pronounced anticancer activity, *Bioorg. Chem.*, 2024, **147**, 107413, DOI: 10.1016/j.bioorg.2024.107413.

19 H. S. H. Mohamed and S. A. Ahmed, Reviewing of Synthesis and Computational Studies of Pyrazolo Pyrimidine Derivatives, *J. Chem. Rev.*, 2019, **1**(3), 183–232.

20 E. K. A. Abdelall, R. B. Bakr, M. K. Abdel-Hamid and M. M. Kandeel, Enhancement to synthesize, design and dock of novel EGFR inhibitors containing pyrazolo[3,4-d] pyrimidine cores of expected anticancer activity, *Org. Chem.: Indian J.*, 2014, **10**(12), 470–483.

21 D. Adel, K. El-Adl, T. Nasr, T. M. Sakr and W. Zaghary, Pyrazolo[3,4-d]pyrimidine derivatives as EGFRT790M and VEGFR-2 dual TK inhibitors: Design, synthesis, molecular docking, ADMET profile and anticancer evaluations, *J. Mol. Struct.*, 2023, **1291**, 136047, DOI: 10.1016/j.molstruc.2023.136047.

22 I. M. Salem, S. M. Mostafa, I. Salama, O. I. El-Sabbagh, W. A. H. Hegazy and T. S. Ibrahim, Design, synthesis and antitumor evaluation of novel pyrazolo[3,4-d]pyrimidines incorporating different amino acid conjugates as potential DHFR inhibitors, *J. Enzyme Inhib. Med. Chem.*, 2023, **38**(1), 203–215, DOI: 10.1080/14756366.2022.2142786.

23 K. Somakala, S. Tariq and M. Amir, Synthesis, evaluation and docking of novel pyrazolo pyrimidines as potent p38α MAP kinase inhibitors with improved anti-inflammatory, ulcerogenic and TNF-α inhibitory properties, *Bioorg. Chem.*, 2019, **87**, 550–559, DOI: 10.1016/j.bioorg.2019.03.037.

24 K. El-Adl, A. -H. Abdel-Rahman, A. M. Omar, M. Alswah and N. M. Saleh, Design, synthesis, anticancer, and docking of some S- and/or N-heterocyclic derivatives as VEGFR-2

inhibitors, *Arch. Pharm.*, 2021, e2100237, DOI: 10.1002/ardp.202100237.

25 V. Gandin, A. Ferrarese, M. Dalla Via, C. Marzano, A. Chilin and G. Marzaro, Targeting kinases with anilinopyrimidines: discovery of N-phenyl-N'-[4-(pyrimidin-4-ylamino) phenyl] urea derivatives as selective inhibitors of class III receptor tyrosine kinase subfamily, *Sci. Rep.*, 2015, **5**, 16750.

26 K. El-Adl, H. Sakr, M. Nasser and F. M. A. Shoman, 5-(4-Methoxybenzylidene)thiazolidine-2,4-dione-derived VEGFR-2 inhibitors: Design, synthesis, molecular docking, and anticancer evaluations, *Arch. Pharm.*, 2020, e2000079, DOI: 10.1002/ardp.202000079.

27 K. El-Adl, A. A. El-Helby, H. Sakr and S. S. A. El-Hddad, Design, synthesis, molecular docking, and anticancer evaluations of 1-benzylquinazoline-2,4(1H,3H)-dione bearing different moieties as VEGFR-2 inhibitors, *Arch. Pharm.*, 2020, e2000068, DOI: 10.1002/ardp.202000068.

28 K. El-Adl, A. A. El-Helby, H. Sakr, I. H. Eissa, S. S. A. El-Hddad and F. M. A. Shoman, Design, synthesis, molecular docking and anticancer evaluations of 5-benzylidenethiazolidine-2,4-dione derivatives targeting VEGFR-2 enzyme, *Bioorg. Chem.*, 2020, **102**, 104059, DOI: 10.1016/j.bioorg.2020.104059.

29 A. M. Sayed, F. A. Taher, M. R. K. Abdel-Samad, M. S. A. El-Gaby, K. El-Adl and N. M. Saleh, Design, synthesis, molecular docking, in silico ADMET profile and anticancer evaluations of sulfonamide endowed with hydrazone-coupled derivatives as VEGFR-2 inhibitors, *Bioorg. Chem.*, 2021, **108**, 104669, DOI: 10.1016/j.bioorg.2021.104669.

30 N. M. Saleh, M. S. A. El-Gaby, K. El-Adl and N. E. A. Abd El-Sattar, Design, green synthesis, molecular docking and anticancer evaluations of diazepam bearing sulfonamide moieties as VEGFR-2 inhibitors, *Bioorg. Chem.*, 2020, **104**, 104350, DOI: 10.1016/j.bioorg.2020.104350.

31 K. El-Adl, A. A. El-Helby, H. Sakr and A. Elwan, Design, synthesis, molecular docking and anti-proliferative evaluations of [1,2,4]triazolo[4,3-a]quinoxaline derivatives as DNA intercalators and Topoisomerase II inhibitors, *Bioorg. Chem.*, 2020, **105**, 104399, DOI: 10.1016/j.bioorg.2020.104399.

32 K. El-Adl, A. A. El-Helby, H. Sakr and A. Elwan, [1,2,4]Triazolo [4,3-a]quinoxaline and [1,2,4]triazolo[4,3-a]quinoxaline-1-thiol-derived DNA intercalators: design, synthesis, molecular docking, in silico ADMET profiles and anti-proliferative evaluations, *New J. Chem.*, 2021, **45**, 881, DOI: 10.1039/D0NJ02990D.

33 N. E. A. Abd El-Sattar, K. El-Adl, M. A. El-Hashash, S. A. Salama and M. M. Elhady, Design, synthesis, molecular docking and in silico ADMET profile of pyrano [2,3-d]pyrimidine derivatives as antimicrobial and anticancer agents, *Bioorg. Chem.*, 2021, **115**, 105186, DOI: 10.1016/j.bioorg.2021.105186.

34 N. S. Hanafy, N. A. A. M. Aziz, S. S. A. El-Hddad, M. A. Abdelgawad, M. M. Ghoneim, A. F. Dawood, S. Mohamady, K. El-Adl and S. Ahmed, Design, synthesis, and docking of novel thiazolidine-2,4-dione multitarget scaffold as new approach for cancer treatment, *Arch. Pharm.*, 2023, e2300137, DOI: 10.1002/ardp.202300137.

35 M. A. El-Zahabi, H. Sakr, K. El-Adl, M. Zayed, A. S. Abdelraheem, S. I. Eissa, H. Elkady and I. H. Eissa, Design, synthesis, and biological evaluation of new challenging thalidomide analogs as potential anticancer immunomodulatory agents, *Bioorg. Chem.*, 2020, **104**, 104218, DOI: 10.1016/j.bioorg.2020.104218.

36 A. E. Abdallah, I. H. Eissa, A. B. M. Mehany, H. Sakr, A. Atwa, K. El-Adl and M. A. El-Zahabi, Immunomodulatory quinazoline-based thalidomide analogs: Design, synthesis, apoptosis and anticancer evaluations. J, *J. Mol. Struct.*, 2023, **1281**, 135164, DOI: 10.1016/j.molstruc.2023.135164.

37 M. A. El-Zahabi, H. Elkady, H. Sakr, A. S. Abdelraheem, S. I. Eissa and K. El-Adl, Design, synthesis, anticancer evaluation, in silico docking and ADMET analysis of novel indole-based thalidomide analogs as promising immunomodulatory agents, *J. Biomol. Struct. Dyn.*, 2023, **41**(24), 15106–15123, DOI: 10.1080/07391102.2023.2187217.

38 F. T. Ali, A. K. Yousef, F. A. Ahmed, F. M. Elgneady, K. El-Adl and M. M. Elhady, *In silico* ADMET, docking, anti-proliferative and antimicrobial evaluations of ethanolic extract of Euphorbia dendroides L, *S. Afr. J. Bot.*, 2022, **150**, 607–620, DOI: 10.1016/j.sajb.2022.08.009.

39 S. El-Hddad, M. Sobhy, A. Ayoub and K. El-Adl, *In silico* molecular docking, dynamics simulation and repurposing of some VEGFR-2 inhibitors based on the SARS-CoV-2-main-protease inhibitor N3, *J. Biomol. Struct. Dyn.*, 2022, 1–15, DOI: 10.1080/07391102.2022.2148000.

40 H. Elkady, K. El-Adl, H. Sakr, A. S. Abdelraheem, S. I. Eissa and M. A. El-Zahabi, Novel promising benzoxazole/benzothiazole-derived immunomodulatory agents: Design, synthesis, anticancer evaluation, and in silico ADMET analysis, *Arch. Pharm.*, 2023, **356**(9), e2300097, DOI: 10.1002/ardp.202300097.

41 Q.-Q. Xie, H. Z. Xie, J. X. Ren, L. L. Li and S. Y. Yang, Pharmacophore modeling studies of type I and type II kinase inhibitors of Tie2, *J. Mol. Graph. Model.*, 2009, **27**(6), 751–758, DOI: 10.1016/j.jmgm.2008.11.008.

42 K. Lee, K. W. Jeong, Y. Lee, J. Y. Song, M. S. Kim, G. S. Lee and Y. Kim, Pharmacophore modeling and virtual screening studies for new VEGFR-2 kinase inhibitors, *Eur. J. Med. Chem.*, 2010, **45**(11), 5420–5427, DOI: 10.1016/j.ejmech.2010.09.002.

43 J. Dietrich, C. Hulme and L. H. Hurley, The design, synthesis, and evaluation of 8 hybrid DFG-out allosteric kinase inhibitors: A structural analysis of the binding interactions of Gleevec®, Nexavar®, and BIRB-796, *Bioorg. Med. Chem.*, 2010, **18**(15), 5738–5748.

44 Z. Wang, N. Wang, S. Han, D. Wang, S. Mo, L. Yu, H. Huang, K. Tsui, J. Shen and J. Chen, Dietary compound isoliquiritigenin inhibits breast cancer neoangiogenesis via VEGF/VEGFR-2 signaling pathway, *PLoS One*, 2013, **8**(7), e68566, DOI: 10.1371/journal.pone.0068566.

45 V. A. Machado, D. Peixoto, R. Costa, H. J. Froufe, R. C. Calhelha, R. M. Abreu, I. C. Ferreira, R. Soares and M. J. Queiroz, Synthesis, antiangiogenesis evaluation and molecular docking studies of 1-aryl-3-[(thieno[3,2-b]pyridin-7-ylthio)phenyl]ureas: Discovery of a new substitution

pattern for type II VEGFR-2 Tyr kinase inhibitors, *Bioorg. Med. Chem.*, 2015, **23**(19), 6497–6509, DOI: 10.1016/j.bmc.2015.08.010.

46 Z. Zhao, H. Wu, L. Wang, Y. Liu, S. Knapp, Q. Liu and N. S. Gray, Exploration of type II binding mode: a privileged approach for kinase inhibitor focused drug discovery?, *ACS Chem. Biol.*, 2014, **9**(6), 1230–1241.

47 S. A. Elmetwally, K. F. Saied, I. H. Eissa and E. B. Elkaeed, Design, synthesis and anticancer evaluation of thieno[2,3-d]pyrimidine derivatives as dual EGFR/HER2 inhibitors and apoptosis inducers, *Bioorg. Chem.*, 2019, **88**, 102944, DOI: 10.1016/j.bioorg.2019.102944.

48 A. A. Gaber, A. M. El-Morsy, F. F. Sherbiny, A. H. Bayoumi, K. M. El-Gamal, K. El-Adl, A. A. Al-Karmalawy, R. R. Ezz Eldin, M. A. Saleh and H. S. Abulkhair, Pharmacophore-linked pyrazolo[3,4-d]pyrimidines as EGFR-TK inhibitors: Synthesis, anticancer evaluation, pharmacokinetics, and in silico mechanistic studies, *Arch. Pharm.*, 2021, e2100258, DOI: 10.1002/ardp.202100258.

49 R. B. A. Bakr, E. K. Abdelallm, M. K. Abdel-Hamid and M. M. Kandeel, design and synthesis of new EGFR-tyrosine kinase inhibitors containing pyrazolo[3,4-d] pyrimidine cores as anticancer agents, *Bull. Pharm. Sci. Assiut Univ.*, 2012, **35**(1), 27–42.

50 F. Khedr, M.-K. Ibrahim, I. H. Eissa, H. S. Abulkhair and K. El-Adl, Phthalazine-based VEGFR-2 inhibitors: Rationale, design, synthesis, in silico, ADMET profile, docking, and anticancer evaluations, *Arch. Pharm.*, 2021, e2100201, DOI: 10.1002/ardp.202100201.

51 N. A. A. M. Aziz, R. F. George, K. El-Adl and W. R. Mahmoud, Design, synthesis, in silico docking, ADMET and anticancer evaluations of thiazolidine-2,4-diones bearing heterocyclic rings as dual VEGFR-2/EGFRT790M tyrosine kinase inhibitors, *RSC Adv.*, 2022, **12**, 12913, DOI: 10.1039/d2ra01119k.

52 N. A. A. M. Aziz, R. F. George, K. El-Adl and W. R. Mahmoud, Exploration of thiazolidine-2,4-diones as tyrosine kinase inhibitors: Design, synthesis, ADMET, docking, and antiproliferative evaluations, *Arch. Pharm.*, 2022, e2200465, DOI: 10.1002/ardp.202200465.

53 B. R. Miller, T. D. J. McGee, J. M. Swails, N. Homeyer, H. Gohlke and A. E. Roitberg, MMPBSA.py: An efficient program for end-state free energy calculations, *J. Chem. Theory Comput.*, 2012, **8**(9), 3314–3321, DOI: 10.1021/ct300418h.

54 J. A. Maier, C. Martinez, K. Kasavajhala, L. Wickstrom, K. E. Hauser and C. Simmerling, ff14SB: improving the accuracy of protein side chain and backbone parameters from ff99SB, *J. Chem. Theory Comput.*, 2015, **11**(8), 3696–3713, DOI: 10.1021/acs.jctc.5b00255.

55 J. Wang, R. M. Wolf, J. W. Caldwell, P. A. Kollman and D. A. Case, Development and testing of a general amber force field, *J. Comput. Chem.*, 2004, **25**(9), 1157–1174, DOI: 10.1002/jcc.20035.

56 S. El-Hddad, M. Sobhy, A. Ayoub and K. El-Adl, *In silico* molecular docking, dynamics simulation and repurposing of some VEGFR-2 inhibitors based on the SARS-CoV-2-main-protease inhibitor N3, *J. Biomol. Struct. Dyn.*, 2022, **41**(19), 9267–9281, DOI: 10.1080/07391102.2022.2148000.

57 T. Mosmann, Rapid colorimetric assay for cellular growth and survival: application to proliferation and cytotoxicity assays, *J. Immunol. Methods*, 1983, **65**(1–2), 55–63.

58 F. M. Freimoser, C. A. Jakob, M. Aebi and U. Tuor, The MTT [3-(4,5-dimethylthiazol-2-yl)-2,5-diphenyltetrazolium bromide] assay is a fast and reliable method for colorimetric determination of fungal cell densities, *Appl. Environ. Microbiol.*, 1999, **65**(8), 3727–3729, DOI: 10.1128/AEM.65.8.3727-3729.1999.

59 M. Ghasemi, T. Turnbull, S. Sebastian and I. Kempson, The MTT Assay: Utility, Limitations, Pitfalls, and Interpretation in Bulk and Single-Cell Analysis, *Int. J. Mol. Sci.*, 2021, **22**(23), 12827, DOI: 10.3390/ijms222312827.

60 L. Benov, Improved Formazan Dissolution for Bacterial MTT Assay, *Microbiol. Spectr.*, 2021, **9**(3), e0163721, DOI: 10.1128/spectrum.01637-21.

61 S. M. Abou-Seri, W. M. Eldehna, M. M. Ali and D. A. Abou El Ella, 1-Piperazinylphthalazines as potential VEGFR-2 inhibitors and anticancer agents: Synthesis and in vitro biological evaluation, *Eur. J. Med. Chem.*, 2016, **107**, 165–179, DOI: 10.1016/j.ejmech.2015.10.053.

62 Y. Jia, C. M. Quinn, A. I. Gagnon and R. Talanian, Homogeneous time-resolved fluorescence and its applications for kinase assays in drug discovery, *Anal. Biochem.*, 2006, **356**(2), 273–281.

63 C. A. Lipinski, F. Lombardo, B. W. Dominy and P. J. Feeney, Experimental and computational approaches to estimate solubility and permeability in drug discovery and development settings, *Adv. Drug Deliv. Rev.*, 1997, **23**(1–3), 3–25, DOI: 10.1016/S0169-409X(96)00423-1.

64 D. E. V. Pires, T. L. Blundell and D. B. Ascher, pkCSM: Predicting Small-Molecule Pharmacokinetic and Toxicity Properties Using Graph-Based Signatures, *J. Med. Chem.*, 2015, **58**(9), 4066–4072, DOI: 10.1021/acs.jmedchem.5b00104.

65 A. Beig, R. Agbaria and A. Dahan, Oral Delivery of Lipophilic Drugs: The Tradeoff between Solubility Increase and Permeability Decrease When Using Cyclodextrin-Based Formulations, *PLoS One*, 2013, **8**, e68237, DOI: 10.1371/journal.pone.0068237.